CHEMISTRY
A EUROPEAN JOURNAL

DOI: 10.1002/chem.201103451

VIP

Ruthenium(II) Photosensitizers of Tridentate Click-Derived Cyclometalating Ligands: A Joint Experimental and Computational Study

Benjamin Schulze,[a, b] Daniel Escudero,[b, c] Christian Friebe,[a, b] Ronald Siebert,[b, d] Helmar Görls,[e] Stephan Sinn,[a, b] Martin Thomas,[b, c] Sebastian Mai,[b, c] Jürgen Popp,[b, d] Benjamin Dietzek,*[b, d] Leticia González,*[b, c, f] and Ulrich S. Schubert*[a, b]

Abstract: A systematic series of heteroleptic bis(tridentate)ruthenium(II) complexes of click-derived 1,3-bis(1,2,3-triazol-4-yl)benzene N^C^N-coordinating ligands was synthesized, analyzed by single crystal X-ray diffraction, investigated photophysically and electrochemically, and studied by computational methods. The presented comprehensive characterization allows a more detailed understanding of the radiationless deactivation mechanisms. Furthermore, we provide a fully optimized synthesis and systematic variations towards redox-matched, broadly and intensely absorbing, cyclometalated ruthenium(II) complexes. Most of them show a weak room-temperature emission and a prolonged excited-state lifetime. They display a broad absorption up to 700 nm and high molar extinction coefficients up to $20000\,M^{-1}cm^{-1}$ of the metal-to-ligand charge transfer bands, resulting in a black color. Thus, the complexes reveal great potential for dye-sensitized solar-cell applications.

Keywords: click chemistry · computational methods · cyclometalation · photosensitizers · ruthenium

Introduction

Ruthenium(II) polypyridyl complexes are highly prominent in photochemistry, since they allow for a light-driven charge separation in which the ligand becomes photoreduced while the metal is photooxidized and both can undergo subsequent redox reactions in terms of artificial photosynthesis. This metal-to-ligand charge transfer (MLCT) can be fine-tuned by the ligand properties to optimize the photophysical and electrochemical properties. To allow homogeneous, diffusion-controlled photocatalysis, a long excited-state lifetime is most important. A central dilemma is that, in contrast to tris(bidentate) ruthenium(II) complexes, bis(tridentate) ones are more stable and allow an isomer-free functionalization, but typically show only short excited-state lifetimes.[1] Various optimization strategies to prolong the excited-state lifetime have been developed.[2] The use of very strong, anionic donors causes slightly prolonged lifetimes, and moreover, interesting properties such as a broadened and red-shifted absorption of visible light and a directed MLCT transition.

An application for which these features become most important and the lifetimes are not that crucial, due to immobilization of the complexes and fast electron injection into the semiconductor, is the dye-sensitized solar cell (DSSC), developed by O'Regan and Grätzel in 1991.[3] The DSSC applies the principles of natural photosynthesis, namely the spatial separation of the basic functions that are light-driven charge separation and charge transport, and, therefore, allows for modular manipulations of the light-harvesting dyes. Here, the almost pure, and thus predictable and tunable MLCT and reversible redox behavior made Ru^{II} polypyridyl complexes the most attractive candidates. In particu-

[a] B. Schulze, C. Friebe, S. Sinn, Prof. Dr. U. S. Schubert
Laboratory of Organic and Macromolecular Chemistry (IOMC)
Friedrich-Schiller-University Jena
Humboldtstr. 10, 07743 Jena (Germany)
Fax: (+49) 3641948202
E-mail: ulrich.schubert@uni-jena.de

[b] B. Schulze, Dr. D. Escudero, C. Friebe, Dr. R. Siebert, S. Sinn, M. Thomas, S. Mai, Prof. Dr. J. Popp, Prof. Dr. B. Dietzek, Prof. Dr. L. González, Prof. Dr. U. S. Schubert
Jena Center for Soft Matter (JCSM)
Friedrich-Schiller-University Jena
Humboldtstr. 10, 07743 Jena (Germany)

[c] Dr. D. Escudero, M. Thomas, S. Mai, Prof. Dr. L. González
Laboratory of Theoretical Chemistry
Friedrich-Schiller-University Jena
Helmholtzweg 4, 07743 Jena (Germany)

[d] Dr. R. Siebert, Prof. Dr. J. Popp, Prof. Dr. B. Dietzek
Institute of Physical Chemistry and Abbe Center of Photonics
Friedrich-Schiller-University Jena
Helmholtzweg 4, 07743 Jena (Germany)
and Institute of Photonic Technology Jena
Albert-Einstein-Straße 9, 07745 Jena (Germany)
Fax: (+49) 3641206399
E-mail: benjamin.dietzek@uni-jena.de

[e] Dr. H. Görls
Laboratory of Inorganic and Analytic Chemistry
Friedrich-Schiller-University Jena
Lessingstr. 8, 07743 Jena (Germany)

[f] Prof. Dr. L. González
Current address: Prof. Dr. L. González
Institute of Theoretical Chemistry, University of Vienna
Währinger Str. 17, 1090 Vienna (Austria)
Fax: (+43) 1427752793
E-mail: leticia.gonzalez@univie.ac.at

Supporting information for this article is available on the WWW under http://dx.doi.org/10.1002/chem.201103451.

WILEY ONLINE LIBRARY

© 2012 Wiley-VCH Verlag GmbH & Co. KGaA, Weinheim

lar, Ru^{II} complexes featuring thiocyanate ligands like the red (N3, N719) and black dyes (N749) still display the benchmark with about 11% solar-cell efficiency.[4] Their anionic, strong σ- and π-donating thiocyanate ligand enables panchromatic absorption and efficient electron injection into the semiconductor. However, at the same time the main drawback of the classical Ru^{II} dyes is the monodentate thiocyanate ligand limiting their stability and prohibiting further functionalization that could improve the light harvesting. Consequently, Ru^{II} complexes possessing aromatic carbanion donors that essentially adopt the function of the thiocyanate have been employed in DSSCs with great success.[5] When embedded within a multidentate ligand, this cyclometalation[6] allows for higher stability and ligand functionalization to optimize the photophysical and electrochemical properties.

Recently, click-derived[7] ligands have been successfully used as analogues of polypyridyl ligands, in particular of 2,2′:6′,2″-terpyridine (tpy).[8] We were interested in extending this analogy to tridentate cyclometalating polypyridyl ligands, namely 1,3-dipyridylbenzene (dpbH).[9] In this context, we present a new and systematic series of click-derived, tridentate, cyclometalated Ru^{II} complexes[10] that was studied in detail by experimental and computational methods to elucidate the potential for dye-sensitized solar-cell application.[11] Thereby, the combination of theoretical investigations and photophysical as well as electrochemical studies enables a consistent and emergent explanatory picture of the new dyes.

Results and Discussion

Syntheses: A fully optimized synthetic procedure is presented for the new cyclometalated complexes as well as for a non-cyclometalated model complex.[8d] The optimization, the design strategy and an exemplary synthetic procedure are explained in the following. For synthetic details, the reader is referred to the Supporting Information.

The ligands were obtained from aryl azides and diethynylbenzene building blocks in good yields using standard click conditions. For the sake of blocking alternative, bidentate coordinations that were observed in initial attempts, methyl groups were placed at strategic positions when possible and reasonable.[12] Therefore, *o*-xylene was chosen as the central ring as well as mesityl moieties for the clicked-on functionalities (Scheme 1).

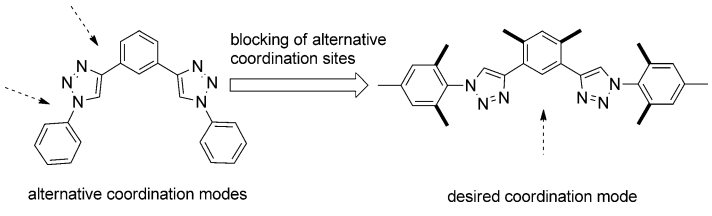

Scheme 1. Schematic illustration of the optimization strategy.

Furthermore, mesityl was chosen as substituent for further reasons: 1) it enables both good solubility and good crystallization behavior, 2) it is electronically decoupled due to its orthogonality and therefore a reasonable electronic reference, 3) it allows for eased NMR interpretations, and 4) it is readily available from mesityl amine through diazotization/azidation and can be considered as a safe azide. The diethynylbenzene building blocks were synthesized under standard Sonogashira conditions with additional LiCl[13] starting from functionalized dibromobenzenes (Scheme 2).

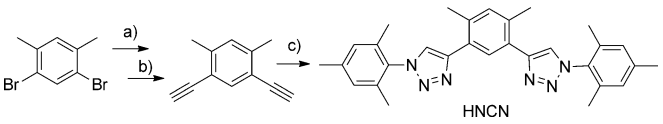

Scheme 2. Exemplary synthesis of the cyclometalating ligands: a) [Pd(PPh_3)$_4$], LiCl, CuI, TMS-CCH, NEt_3, PhMe, 50°C, 72 h; b) KF, THF/MeOH (1:1); 50% over 2 steps; c) $CuSO_4 \cdot 5H_2O$, NaAsc., $MesN_3$, CH_2Cl_2/EtOH/H_2O (1:2:1), 60°C, 12 h, 90%.

In one case, σ-accepting fluoro substituents replace the methyl groups in the position *meta* to the carbanion to allow blocking as well as electronic fine-tuning.[5c,e,12] In the case of 1,3,5-tribromobenzene, 2-methylbut-3-yn-2-ol was chosen as protected alkyne to ease the chromatographic separation.[14] After deprotection and cycloaddition, the according 5-bromo-1,3-bis(triazolyl)benzene allows further ligand-functionalizations by cross-coupling methods in an important position. The subsequent installation of a chromophore at the *para* position of the cyclometalating ring, for example, thiophene, would extend the conjugated system and increase the light absorptivity. Similarly, the mesityl azide reference was changed once to 9-(4-azidophenyl)-3,6-di-*tert*-butyl-9*H*-carbazole to install an organic chromophore at the complex periphery as light-harvesting antenna.[15] In this case, the conjugation through the triazole ring is not expected[16] and the increase of light harvesting would be additive only. However, although click chemistry provides facile functionalization within the ligand formation, leading to modular and higher functionalized complexes, we kept the mesityl moiety as reference in all other cases to discuss the more pronounced influences of substituents directly attached to the cyclometalating phenyl ring or the opposed ligand (Scheme 3). In addition, it is questionable if the overall device efficiency profits from the increased absorptivity due to the carbazoles or if it drops due to lowered dye coverage on the semiconductor surface.

To facilitate the coordination and cyclometalation, the common [Ru^{III}(tpy)Cl_3] precursor can be activated in situ by halide abstraction with a silver(I) salt in a weakly coordinating solvent. However, it is known that silver(I) can oxidize the product yielding a homocoupled dimer[9a] and therefore needs to be filtered off after the activation step. Still, application of a Ru^{III} precursor includes a reduction step towards Ru^{II} after coordination that is normally achieved by alcohols or amines. Since the cyclometalated complexes are oxidized

 © 2012 Wiley-VCH Verlag GmbH & Co. KGaA, Weinheim

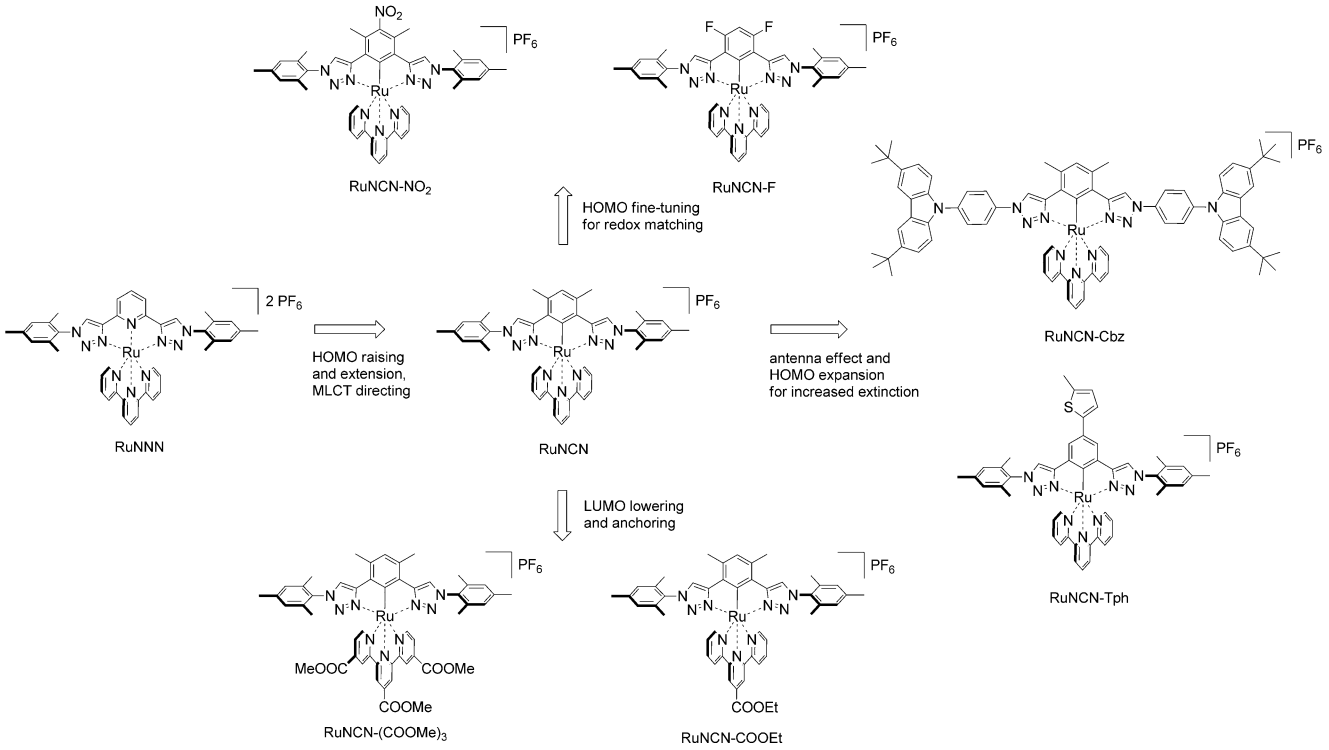

Scheme 3. Design strategy and overview of the synthesized ruthenium(II) complexes.

easily, the product is achieved either as Ru^{III} complex or it already underwent side reactions in the position *para* to the cyclometalation that has significant radical character within the Ru^{III} complex. This drawback can be overcome by the use of $[Ru^{II}(tpy)(CH_3CN)_3][PF_6]_2$ as precursor (see Scheme 4 for a representative example).[17] In fact, it is

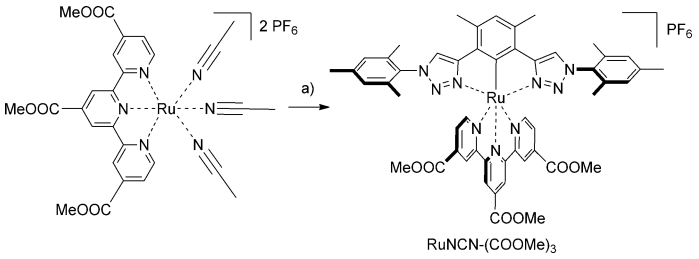

Scheme 4. Exemplary synthesis of the cyclometalated ruthenium(II) complexes: a) HNCN, methanol, microwave, 30 min., 160 °C, 50 %.

easily synthesized from $[Ru^{III}(tpy)Cl_3]$ in acetonitrile/ethanol/water using $AgNO_3$ and, in contrast to $[Ru^{III}(tpy)Cl_3]$, it can be purified completely, thus simplifying the subsequent complexation. In more detail, after removal of the AgCl by filtration over celite, the product can be isolated either by column chromatography or directly by vapor diffusion of diethyl ether into a concentrated acetonitrile solution yielding large, even X-ray-quality crystals (see the Supporting Information). The subsequent cyclometalation was performed under oxygen-free conditions in a closed vial using an alcohol as solvent and microwave heating to 160 °C for 30 min. Isolation of the product by a combination of column chromatography and crystallization afforded the desired complexes, in most cases as X-ray-quality crystals (Figure 1 and the Supporting Information) and in reasonable yields varying from 40 to 70 % (Scheme 4 and the Supporting Information), depending, amongst others, on whether all strategic methyl groups were present.

Since cyclometalated complexes are very electron-rich in the position *para* to the carbanion, they enable targeted homocoupling and post-complexation functionalizations in the presence of oxidants, electrophiles, or both.[18] This allowed the introduction of a nitro group under Menke conditions and, thereby, the respective manipulation of the carbanion donation by a σ- and π-accepting group in turn.[5d]

The installation of the anchoring carboxylic acid functions for the DSSC was achieved simply by using ester functionalized ligands and saponification[5e,f] subsequent to the complexation. Thus, the intermediate, highly soluble, ester-functionalized complexes could be purified and studied, since they are seen as models for the final complexes adsorbed to TiO_2.[5k]

Crystal structures: Single crystals of the ligands HNCN and HNCN-F as well as of the three Ru^{II} precursors and of RuNNN, RuNCN, RuNCN-NO_2, RuNCN-F and RuNCN-Tph could be grown and characterized successfully by X-ray diffraction (Figure 1 and the Supporting Information). The systematic variation allows for comparison although only

 © 2012 Wiley-VCH Verlag GmbH & Co. KGaA, Weinheim

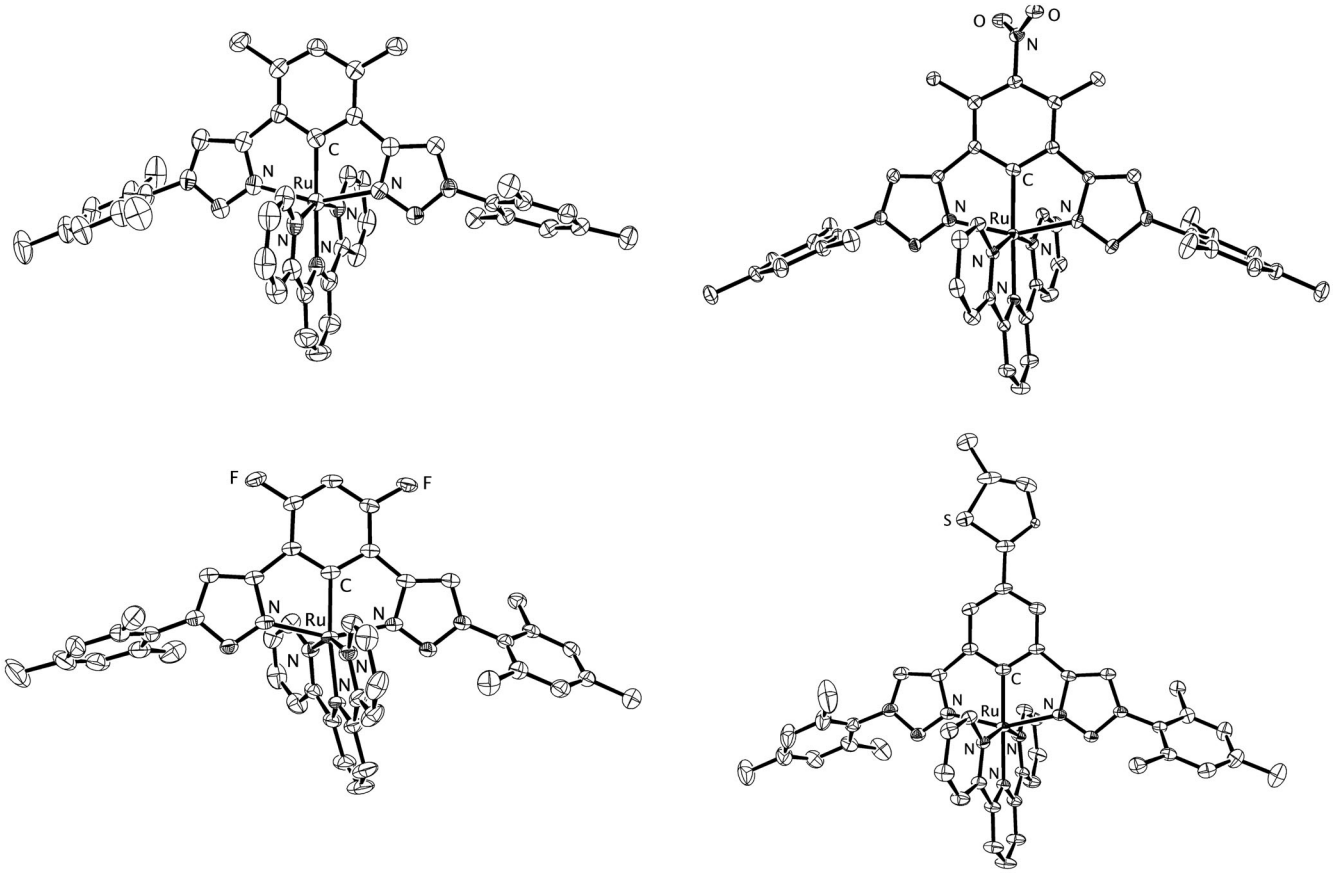

Figure 1. Solid-state structures of RuNCN (top left), RuNCN-NO_2 (top right), RuNCN-F (bottom left) and RuNCN-Tph (bottom right) (50% probability level; counterions, hydrogen atoms and solvent molecules omitted for clarity).

the most pronounced changes are discussed to beware of packing effects (note the strong distortion within RuNCN-F).

The mesityl–triazole torsion angle of the complex series varies between 60° and 90°. The thiophene–phenyl torsion angle in RuNCN-Tph was determined to be 30.7°, thus being in good agreement with the calculated value of 30.2° (see Scheme S9 in the Supporting Information) and allowing for partial extension of the conjugation into the thiophene ring.

The replacement of a dative Ru–N bond of the polypyridyl-type complex RuNNN by a covalent, organometallic Ru–C bond within the cyclometalated RuNCN complex leads to a bond shortening from 2.02 to 1.98 Å, caused by the very good σ donation and additional π donation as well as by electrostatic interactions with the anionic, aromatic carbon donor. Furthermore, the adjacent triazole N–Ru bonds are slightly elongated, most likely due to a declined σ orbital overlap by the smaller bite angle. As a consequence of the good electron donation ability of the carbanion, the opposed Ru–N bond becomes elongated from 1.97 to 2.01 Å which is well-known as *trans* influence. Furthermore, the outer pyridine N–Ru bonds are shortened as result of increased π back donation from the more electron-rich Ru^{II} metal center in the cyclometalated complex (Figure 2 and Scheme 5). Also within the triazole ring, the N^2–N^3 double bond is elongated as a consequence of the increased π back donation into π* orbitals.

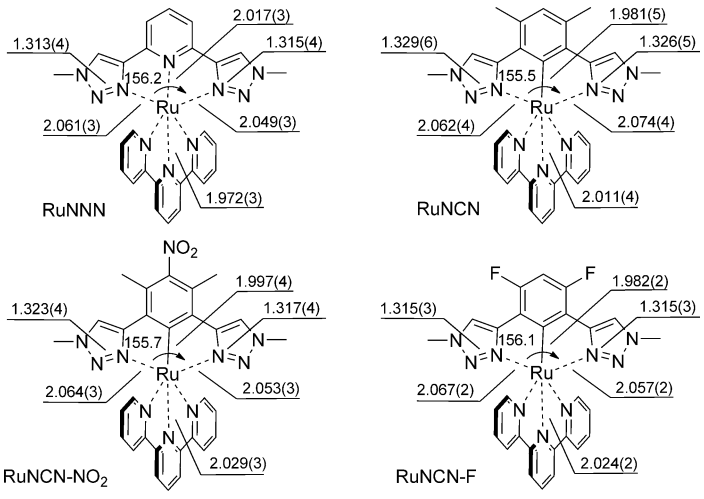

Figure 2. Selected bond lengths (Å) and angles (°) of RuNNN, RuNCN, RuNCN-NO_2 and RuNCN-F.

For RuNCN-NO_2, upon installing an electron-withdrawing group, namely a nitro group that is capable of withdrawal

 © 2012 Wiley-VCH Verlag GmbH & Co. KGaA, Weinheim

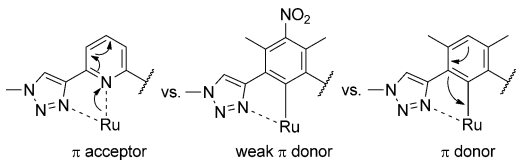

Scheme 5. Schematic representation of the electronic consequences of the cyclometalation and an electron-withdrawing group.

through the σ and π system, most of the consequences of the cyclometalation are less pronounced than for RuNCN. Even though the π-accepting capability might be reduced due to the dihedral angle of 51.8° (51.6° calculated, see Scheme S9 in the Supporting Information) with the central phenyl ring due to repulsion with the *ortho*-methyl groups, there is a distinct influence on the π system that strongly reduces the π-donation ability of the cyclometalating carbanion in the *para* position. Consequently, the Ru–C bond is elongated to 2.00 Å (Figure 2 and Scheme 5). In particular in comparison to RuNCN-F, the fluoro substituents that are strongly σ-accepting, but whose moderate π-donation ability does not affect the carbanion because they are in *meta* positions, still allow a very short Ru–C bond of 1.98 Å. Also the changes in bond lengths within the central phenyl ring are consistent with a participation of a chinoid resonance structure in RuNCN-NO_2. The successive reduction of the electron donation of the carbanion by the fluoro and nitro substituents is demonstrated by the shortening of the triazole N^2=N^3 double bond due to decreased π back donation. Also the Ru–N bond *trans* to the carbanion is further elongated for the same reason.

Apparently, the fluoro substituent mostly influences the σ donation and might lower the energy of the π system indirectly (inductive effect), while the nitro group causes an additional polarization of the π system that strongly weakens the π donation (mesomeric effect) but to a less extent the σ donation. This is consistent with the electrochemical data: for RuNCN-F only the HOMO is stabilized, located on the Ru^{II} metal center and the fluoro-substituted cyclometalating phenyl ring as well, while RuNCN-NO_2 shows an additional LUMO stabilization that is mediated through the aromatic π system/Ru^{II} d orbitals, since the LUMO is located on the opposed tpy ligand.

Interestingly, within all investigated solid-state structures of triazole-containing ruthenium(II) complexes (see Figure S143 in the Supporting Information), short-contact interactions of the triazole with either the counterions or the solvent are present. Triazoles and triazolium salts are known to allow hydrogen bonding as well as electrostatic interactions.[19] Similar to triazolium salts, a ruthenium-coordinated triazole is expected to be more polarized than a free triazole. Preliminary results indicate an interaction of the ruthenium(II)-coordinated triazole with iodide (see Figure S144 in the Supporting Information). The question, if hydrogen bonds/electrostatic interactions might allow the preorganization of the redox mediator in a position favorable for ruthenium(III) reduction, will be targeted in the future.

DFT calculations: As a basis for a deeper understanding of the photophysical and electrochemical properties of the presented Ru^{II} complexes, namely to gain insight into detailed structure–property relations, density functional theory (DFT) calculations, and time-dependent (TD) DFT calculations have been performed.

Whilst the description of the UV/Vis characteristics of these complexes is nowadays close to routine, the description of non-adiabatic events occurring after light excitation is more troublesome. Their description would in principle require the use of multiconfigurational methods in combination with a proper description of spin-orbit coupling (SOC) effects. Unfortunately, these methods are practically unaffordable for Ru^{II}–polypyridyl dyes.[20] Therefore, Δ-SCF-DFT (SCF = self-consistent field) and TDDFT methods remain as valuable alternatives to obtain qualitative and even quantitative information about Ru^{II} complexes and many examples are found in the literature.[21] DFT calculations provide the geometries and energies of the ground and lowest excited states of each symmetry and spin, whilst information on the higher excited states (i.e., energies, oscillator strengths and associated character of the excitations) can be obtained with the help of TDDFT calculations.

In order to understand the deactivation mechanisms after light excitation for RuNNN and RuNCN, their most relevant structures involved, namely the singlet ground state (S_0) as well as the most stable ^{3}MLCT and triplet metal-centered (^{3}MC) excited state, were optimized. As known for Ru^{II}–polypyridyl complexes, after excitation of the ^{1}MLCT manifold, ultrafast inter-system crossing (ISC) occurs within less than 100 fs, leading to the formation of the ^{3}MLCT states with near-unity quantum yield. Among the subsequent radiative and non-radiative processes, radiationless deactivation through thermal population of ^{3}MC states is supposed to determine the ^{3}MLCT lifetime.[1,2] Thus, in addition to the location of the ^{3}MLCT and ^{3}MC states, crossing points between the S_0 and the ^{3}MC potential energy surface determine the non-adiabatic population transfer, as has been recently stated by Boggio-Pasqua et al. for similar Ru^{II}–polypyridyl complexes.[22]

The electronic nature of the lowest-energy triplet excited states of RuNCN has been confirmed by analysis of the spin density distributions (Figure 3). The most stable ^{3}MLCT state indeed displays unpaired electrons within a Ru $4d_{yz}$ orbital and a π* orbital of the tpy ligand, while only Ru-based 4d orbitals are involved in the ^{3}MC state. The main geometrical features of both the optimized ^{3}MLCT and ^{3}MC structures for RuNNN and RuNCN are given in Scheme S9 and S10 in the Supporting Information. In comparison to the S_0 geometry, the ^{3}MLCT and also the ^{3}MC geometries of each complex show a weakening of the coordination, attributed to the population of antibonding orbitals, either π* or "e_g*", as well as to the weakened π back bonding with the formally oxidized Ru "t_{2g}" orbitals. In the ^{3}MC structures the tpy coordination is even distorted (see exemplarily the ^{3}MC structure of RuNCN in Figure 3) due to the weakening, not only of the π back donation but also of the σ donation by the

 © 2012 Wiley-VCH Verlag GmbH & Co. KGaA, Weinheim

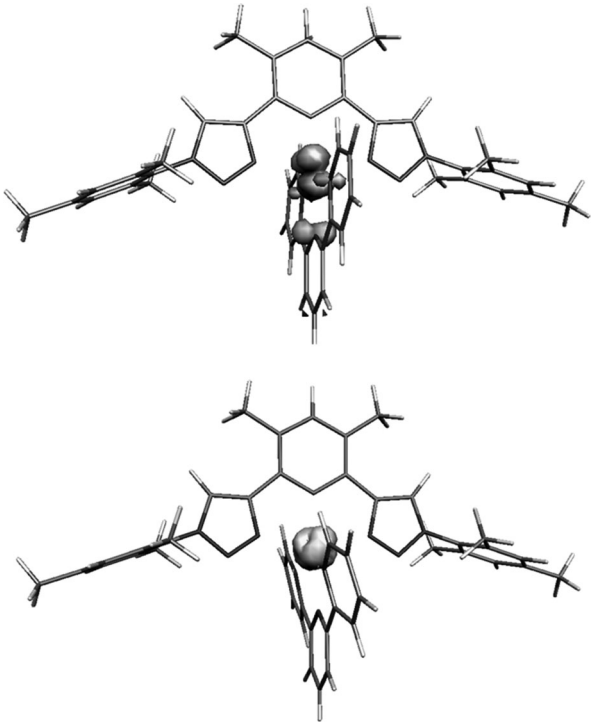

Figure 3. Spin density distribution of the energy optimized ^{3}MLCT (top) and ^{3}MC (bottom) geometries of RuNCN.

population of the "e_g*" levels. Thus, repulsive interactions are avoided by ligand distortion, hence lowering the energy of the ^{3}MC state. This is important, since in the ^{3}MLCT geometry, due to the strong effective σ donation, the unoccupied, antibonding metal d orbitals are located at high energies (see below and Figure 4), while in the ^{3}MC geometry, in which these orbitals are occupied, the destabilizing effects are less pronounced (see the photophysical model section below). Furthermore, while the tridentate ligand is only distorted, a monodentate ligand, such as thiocyanate, can be cleaved off. For all other compounds, only the S_0 and the lowest ^{3}MLCT states were optimized and the main geometrical features are given in the Supporting Information.

To understand the substituent effects on the photophysical properties, the relevant frontier Kohn–Sham orbitals are plotted in Figure 4. For RuNCN, π donation destabilizes the HOMO that is composed of Ru d_{yz} and NCN π orbitals. In contrast, for RuNNN the HOMO is less destabilized and almost of pure Ru d_{xz} character; only a weak π donation contributes to the HOMO−1, which is therefore lower in energy. In both complexes, the LUMO is formed by the same π* orbital of the tpy ligand; however, the strongly destabilized HOMO of RuNCN causes an additional indirect LUMO destabilization through the π back donation. Because the LUMO destabilization is less pronounced than for the HOMO, the resulting energy gap is much smaller for RuNCN. A further effect of the strong electron donation within RuNCN is the strongly destabilized "e_g*" orbitals in terms of a strong ligand field. Thus, the d_{z^2} orbital is the LUMO+8 in RuNNN, being 1.9 eV higher in energy than the LUMO, while in RuNCN it is the LUMO+14 with an energy difference of 2.3 eV. This demonstrates that cyclometalation indeed enables destabilization of orbitals that are populated in ^{3}MC states and that are relevant for the radiationless deactivation. However, the actual electronic situation at the ^{3}MC geometry might be different as mentioned above. Therefore, although the ^{3}MC stabilization might be

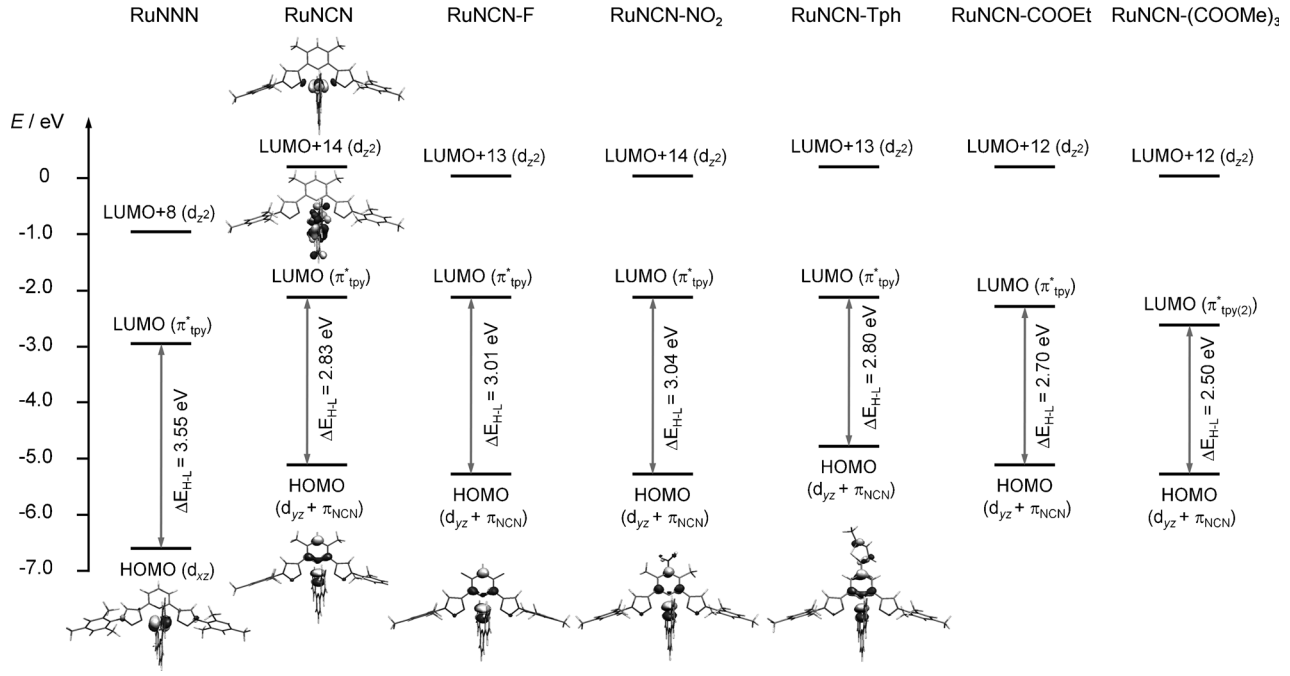

Figure 4. Selected PCM-B3LYP/6-31G* Kohn–Sham orbitals and energy level scheme for the Kohn–Sham orbitals of the Ru^{II} complexes.

 © 2012 Wiley-VCH Verlag GmbH & Co. KGaA, Weinheim

helpful, it does not necessarily cause a suppression of the thermal population of the ^{3}MC from the ^{3}MLCT states (this issue will be discussed in more detail in the photophysical model section below).

Figure 4 also shows the HOMO orbitals of RuNCN-F, RuNCN-NO_2 and RuNCN-Tph. The introduction of an electron-withdrawing fluoro or nitro group directly attached to the HOMO site leads to HOMO stabilization, since the electronic repulsion and electron donation of the carbanion donor is tempered, but also because the aromatic system, which forms a part of the HOMO itself, is stabilized. In case of RuNCN-Tph, the HOMO and LUMO are slightly destabilized due to electron donation from the thiophene moiety, while the energy gap remains constant. Importantly, the conjugation of the HOMO is extended onto the thiophene ring, which should give rise to an increased light absorptivity (see the photophysical properties). Apparently, stabilization due to extension of the conjugation is overcompensated by electron donation of the thiophene. For complexes of ester-functionalized tpy ligands, the HOMO is slightly stabilized because of the increased π acidity of the ligand. Since they are directly attached to the LUMO site, the LUMO level is strongly stabilized by their electron withdrawal, resulting in smaller energy gaps, in particular for RuNCN-$(COOMe)_3$. Furthermore, the LUMO, which is not shown for these complexes, is the same orbital throughout the whole series and differs only in energy. As an exception, in RuNCN-$(COOMe)_3$ the LUMO is a different orbital that is however located on the tpy ligand.

Photophysical properties: A key feature of designated photo-redoxactive Ru^{II} complexes, in particular when aiming at a potential application in dye-sensitized solar cells, is their photophysical behavior. Thus, UV/Vis absorption and emission spectrum measurements as well as photoluminescence quantum yield (Φ_{PL}) and lifetime determinations were executed. Additionally, PCM-TD-B3LYP (PCM = polarizable continuum model) vertical excitations were computed for all the complexes except for RuNCN-Cbz (see the Supporting Information for computational details).

First of all, the free cyclometalating ligands were characterized. Their UV/Vis spectra show a strong absorption peak at around 240 nm with extinction coefficients of 36000–140000 $M^{-1}cm^{-1}$. Additional bands are located at about 295 nm with weak intensities of 1100 and 4600 $M^{-1}cm^{-1}$ for HNCN and HNCN-F, respectively. In contrast, HNCN-Cbz and HNCN-Tph, possessing additional chromophores, exhibit strong absorption peaks beyond 290 nm, with ε values of 58000 and 46300 $M^{-1}cm^{-1}$ for HNCN-Cbz and 15400 $M^{-1}cm^{-1}$ for HNCN-Tph. All ligands are fluorescent, showing emission bands at 325 (HNCN, HNCN-F), 367 (HNCN-Tph), and 404 nm (HNCN-Cbz) (see the Supporting Information).

The absorption and emission features as well as the computed transitions of the studied Ru^{II} complexes are shown in Figure 5 and Table 1. For the assignment of the PCM-TD-B3LYP excitations, see Tables S4–S10 in the Supporting Information. Firstly, the comparison of the parent cyclometalated complex RuNCN with its non-cyclometalated counterpart RuNNN reveals the strong influence of the carbanion donor on the UV/Vis absorption properties. A significant bathochromic shift of the MLCT maxima from 428 to 532 nm, corresponding to 4500 cm^{-1}, is observed upon cyclometalation and well reproduced by the performed calculations. Additionally, an extension of the absorption from 550 to 650 nm is observed that can be explained by destabilization of the Ru-4d orbitals in the RuNCN complex. Indeed, the electronic excitations responsible for these bands involve mainly these orbitals (Table S4 in the Supporting Information). Furthermore, since RuNCN possesses an organometallic, covalent bond, the HOMO is composed of Ru-d orbitals as well as π orbitals of the cyclometalating ligand, while the LUMO (and higher unoccupied molecular orbitals) is π*-tpy-based. Thus, if the anchoring groups are installed at the tpy acceptor ligand, the transition dipole moment is directed towards the semiconductor surface by the distinct push–pull effect.[5a] Since these transitions exhibit partial ligand-to-ligand charge-transfer (LLCT) character, they can be described as metal/ligand-to-ligand charge-transfer (MLLCT) excitations. This underlines the feasibility of directly influencing the HOMO by manipulation of the cyclometalating ligand, although usually the MLCT declaration is kept in literature.[5f,j] Furthermore, the MLCT bands are broadened and even split because of the electronic asymmetry that breaks the orbital degeneracy. Thus, the shorter wavelength transitions around 400 nm exhibit MLCT, MLLCT, and admixed MC character (see S_6, S_{14} and S_{17} in Table S4 in the Supporting Information). In the UV region, the high-energy transitions are mainly of π–π* character (see S_{34} and S_{41}). However, after thermal relaxation in terms of Kasha's rule, the transferred charge will reside on the acceptor ligand. As a further result of the strong anionic carbon donor, a weak room-temperature emission at 751 nm (Φ_{PL}: 0.006 %) was observed for RuNCN (see the photophysical model below).[6a]

To understand the influence of the triazole moiety, a comparison referring to the corresponding Ru^{II} complexes of pyridine analogues, namely 2,2′:6′,2″-terpyridine and 1,3-dipyridylbenzene, is helpful. When compared to $[Ru(tpy)_2][PF_6]_2$, the analogous but heteroleptic RuNNN shows a broadened and blue-shifted absorption. Also the emission at 77 K, which is similar in shape for both, is blue-shifted from 603 to 574 nm. According to the calculations, the emitting state is of ^{3}MLCT character and tpy-based (see the DFT calculation above). Additionally, the computed emission maxima (adiabatic emission energies obtained with Δ-SCF approach, see the Supporting Information for details), are given in Table 1 and correlate well with the experimental data. The absorption spectra of $[Ru(tpy)(dpb)]PF_6$ and RuNCN are similar,[5j] except for a slight hypsochromic shift that is observed in the absorption and emission spectra of RuNCN. Interestingly, although still weak, the emission is slightly increased for RuNCN, most likely because of the higher emission energy in accordance with the energy-gap

 © 2012 Wiley-VCH Verlag GmbH & Co. KGaA, Weinheim

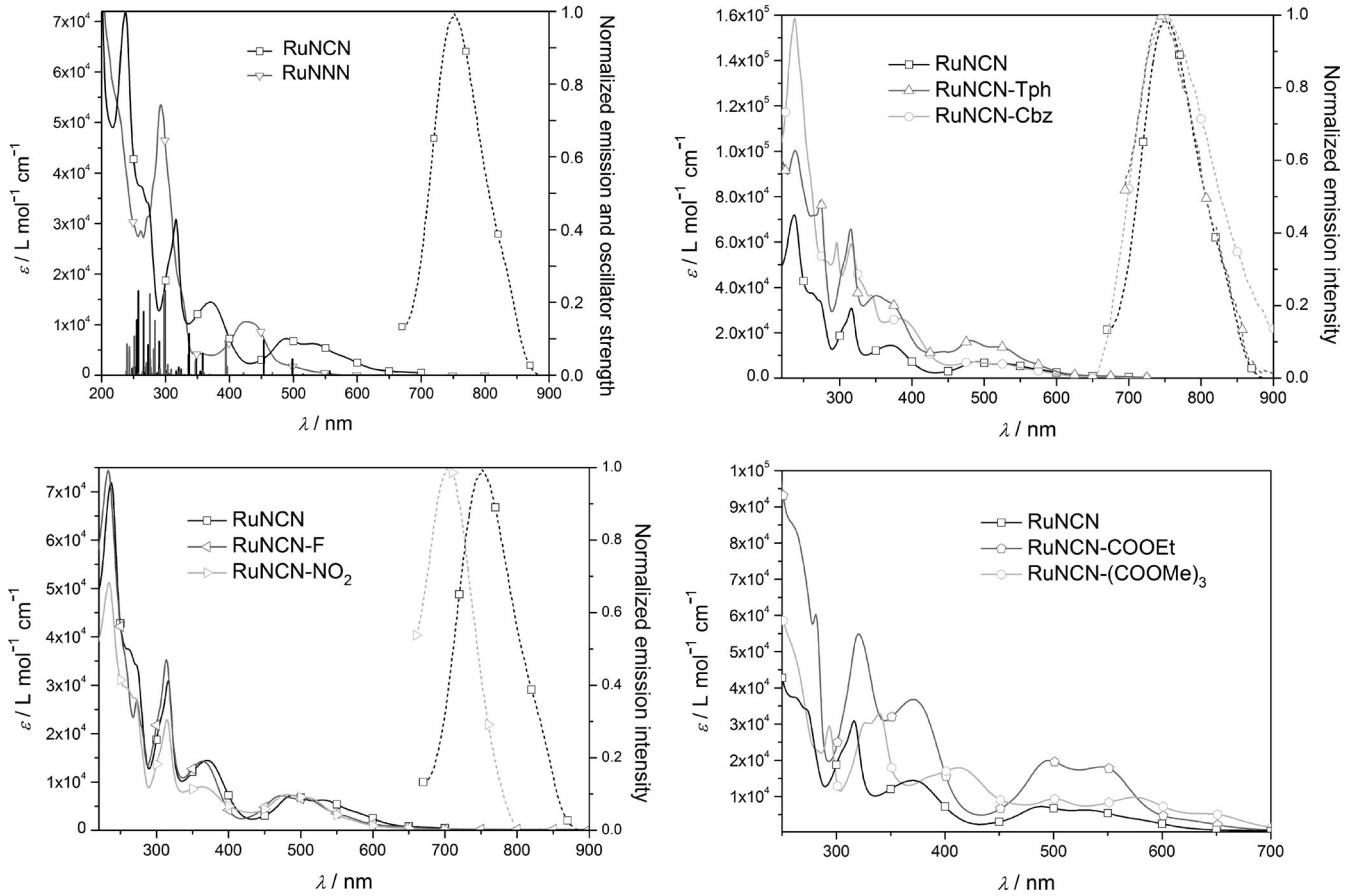

Figure 5. UV/Vis absorption and emission spectra of the investigated ruthenium(II) complexes (10^{-6} M in CH_3CN). For RuNCN and RuNNN, the PCM-TD-DFT/6-31G* computed vertical excitations are superimposed. Solid lines represent the measured curve and symbols are only used for assignment.

law. Furthermore, the extinction coefficients are lowered for RuNCN, attributed to the shorter conjugation that is only partially extended into the triazole.[8a]

To allow for HOMO fine-tuning (see the electrochemical properties below), electron-withdrawing groups, namely nitro and fluoro substituents, were installed at the central phenyl ring. Consequently, a slight hypsochromic shift (700 cm^{-1}) of the MLCT features in the UV/Vis absorption spectrum was observed due to HOMO stabilization. Accordingly, a room-temperature emission can be observed for RuNCN-NO_2 that is blue-shifted by 870 cm^{-1} (Φ_{PL}: 0.010%). In contrast, RuNCN-F features no measurable photoluminescence (see the temperature-dependent lifetime measurements below). Besides, the π-accepting nitro group, *para* to the Ru–C bond, leads to a decrease of the extinction coefficient by a third compared to the parent RuNCN complex, attributed to interference with the push–pull polarization.

To increase the extinction coefficients, additional chromophores were attached[5d–g,15,23] either directly to the central phenyl ring or as clicked-on antennas. The thiophene moiety that was installed *para* to the Ru–C bond increases the extinction coefficients over the whole UV/Vis absorption spectrum, including the highest wavelength absorption that grows from 7300 $M^{-1}cm^{-1}$ for RuNCN to 16500 $M^{-1}cm^{-1}$. Evidently, this is due to extension of the HOMO and, thus, expansion of the optical cross section (see DFT calculations and Figure 4).[5d] In contrast, the attachment of the carbazole moiety provides an additional but separated chromophore that is not in conjugation with the cyclometalated phenyl ring.[16] Thereby, the extinction coefficients below 450 nm double with respect to RuNCN, because the carbazole participates in LC transitions, while the absorption bands beyond 450 nm, in analogy to RuNCN assigned mainly to $d_{Ru}/\pi_{NCN} \rightarrow \pi^*_{tpy}$ transitions, remain unchanged in shape and intensity. Furthermore, the room-temperature emission of RuNCN was preserved, thus no additional quenching pathways are introduced; instead, the emission intensity was even slightly increased (Table 1).

For the immobilization on the semiconductor surface in DSSCs, carboxylic groups on the acceptor ligand are necessary. Beside their function as anchoring groups, they also strongly influence the photophysical properties as additional electron-withdrawing groups. Here, the ester-functionalized complexes were seen as models for the TiO_2-bound dyes.[5k] The introduction of a single carboxylic ester at the 4′-position of the terpyridine causes a stabilization of the π^*_{tpy}-based LUMO (Figure 4) and an enhanced transition dipole moment, thus leading to a slight bathochromic shift by about 500 cm^{-1} as well as a tripled extinction coefficient in

 © 2012 Wiley-VCH Verlag GmbH & Co. KGaA, Weinheim

Table 1. Photophysical data of the complexes.

Complex	298 K				77 K		k_r+k_1	k_2	k_3	ΔE_2	ΔE_3
	λ_{max}^{abs} [nm] (ε [10^3 M^{-1}·cm^{-1}])[a,b]	λ_{max}^{em} [nm][a,c,d]	Φ_{PL} 10^{-5}[a,e]	τ [ns]	λ_{max}^{em} [nm][d]	τ [μs]	[s^{-1}][f]	[s^{-1}]	[s^{-1}]	[cm^{-1}]	[cm^{-1}]
RuNNN	325 (sh), 428 (10.6), 500 (1.8)	– (545)	–	–	574	14	–	–	–	–	–
$[Ru(tpy)_2][PF_6]_2$[5j,30]	308 (63.4), 475 (14.7)	–	–	0.25	603	–	6.5×10^4	2.0×10^{13}	2.1×10^7	1700	720
RuNCN	371 (14.5), 488 (7.3), 532 (6.3)	751 (827)	6.1	4.1	719	4.1	2.44×10^5	1.1×10^{12}	3.11×10^8	1830	350
$[Ru(tpy)(dpb)]PF_6$[5j]	424 (9.6), 499 (14.4), ≈540 (≈10)	781	0.9	–	–	–	–	–	–	–	–
$[Ru(ttpy)(dpb)]PF_6$[g]	504 (10.8), 550 (8.3)	784	4.5	4.5	752	0.48	–	–	–	–	–
RuNCN-F	363 (14.3), 473 (7.2), 507 (6.5)	–	–	0.5[h]	661	5.8	1.72×10^5	9.74×10^{11}	–	1290	–
RuNCN-NO_2	365 (9.0), 483 (7.4), 511 (6.8)	705 (759)	10.0	5.3	667	5.2	1.92×10^5	6.63×10^{11}	–	1395	–
RuNCN-Cbz	384 (26.2), 485 (7.3), 523 (6.3)	750	25.0	6.7[h]	712	4.5	2.22×10^5	2.04×10^{11}	1.33×10^8	1570	270
RuNCN-Tph	350 (36.4), 482 (16.5), 518 (13.8)	745 (802)	5.3	4.1[h]	722	4.3	2.33×10^5	1.89×10^{11}	1.42×10^8	1452	240
RuNCN-COOEt	372 (36.8), 495 (19.9), 546 (18.2)	– (941)[d]	–[d]	–[d]	–[d]	–[d]	–	–	–	–	–
RuNCN-COOH	373 (22.0), 491 (10.5), 532 (10.5)	–	–	12.3	745	5.7	1.75×10^5	2.02×10^{10}	–	1135	–
RuNCN-$(COOMe)_3$	413 (17.9), 500 (9.4), 574 (9.8), 641 (5.3)	– (1032)[d]	–[d]	–[d]	–[d]	–[d]	–	–	–	–	–
RuNCN-$(COOH)_3$	398 (8.7), 497 (5.0), 572 (5.3), 641 (3.2)	–[d]	–[d]	–[d]	–[d]	–[d]	–	–	–	–	–

[a] Measured 10^{-6} M in deaerated CH_3CN. [b] sh = shoulder. [c] In brackets: Adiabatic emission energy values (ΔSCF-PCM-DFT/6-31G*). [d] The detector limit is at 800 nm. [e] Determined using $[Ru(dqp)_2][PF_6]_2$ in MeOH/EtOH (1:4; $\Phi_{PL}=2.0\,\%$)[31] as a reference. [f] The sum of k_r and k_1 is the reciprocal of the 77 K lifetime. [g] ttpy = 4′-tolyl-tpy, from reference [32], note that the 4′-tolyl substituent stabilizes the ^{3}MLCT and thereby prolongs the excited state lifetime.[33] [h] Extrapolated from the temperature-dependent phosphorescence lifetime measurements.

the visible region. When carboxylic ester groups are attached to the *para* positions of all three pyridine moieties of the terpyridine ligand, namely for RuNCN-$(COOMe)_3$, the absorption is again significantly red-shifted (by 3000 cm^{-1}) and additionally broadened, hence covering almost the whole visible spectrum and causing a black color of the complex. The main visible absorption features are slightly more intense and separated, but they reflect the same transitions as in RuNCN, which becomes evident in comparison to a 77 K excitation spectrum of RuNCN (see Figure S118 in the Supporting Information). A photoluminescence of the complexes bearing carboxylic ester groups was not observed, most likely due to the low energy gap according to the energy-gap law (see below) or the reduced spectrometer sensitivity at low emission energies.[24] The drop in extinction and the slight blue shift of the saponified complexes, RuNCN-COOH and RuNCN-$(COOH)_3$, are attributed to the lowered electron acception that causes a decreasing polarization and LUMO stabilization.

77 K emission spectroscopy: As all presented coordination compounds show either no or only a weak emission at room temperature, owing to the presence of several non-radiative deactivation pathways that will be discussed in detail later, the exact energy of the lowest-lying excited state is challenging to determine. Emission spectroscopy at low temperatures can enable the determination of these energies if the dominant non-radiative channels are thermally activated.

All the investigated complexes, except RuNCN-COOEt, RuNCN-$(COOH)_3$ and RuNCN-$(COOMe)_3$, are emissive at 77 K and show bandshapes typical for ruthenium coordination compounds, namely an intense 0–0 transition that is accompanied by a weaker vibronic satellite (Figure 6, see Fig-

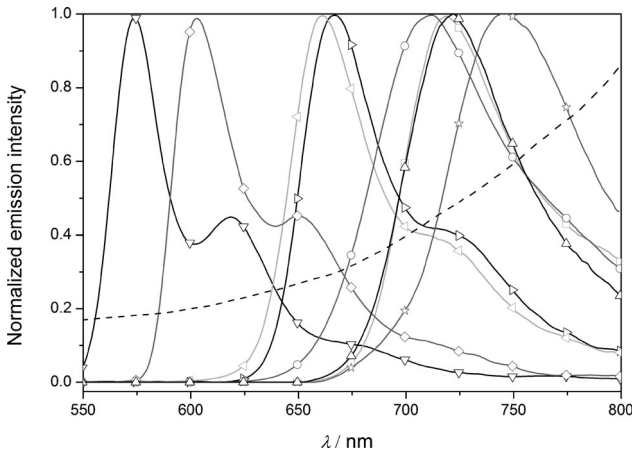

Figure 6. Emission spectra of the complexes: RuNNN (▽), $[Ru^{II}(tpy)_2]$ (◇), RuNCN-F (◁), RuNCN-NO_2 (▷), RuNCN-Cbz (○), RuNCN (□), RuNCN-Tph (△) and RuNCN-COOH (☆) in *n*-butyronitrile glass at 77 K. The spectral resolution decreases at higher wavelengths due to a decreasing spectrometer sensitivity (spectrometer response is given as a dashed line). Solid lines represent the measured curve and symbols are only used for assignment, a color figure is given in the Supporting Information (Figure S119).

 © 2012 Wiley-VCH Verlag GmbH & Co. KGaA, Weinheim

ure S118 in the Supporting Information for excitation spectra). The emission maxima are summarized in Table 1. We note that the emission at 77 K is blue-shifted compared to the respective room-temperature emission, because the rigid solvent matrix at low temperatures prevents solvent reorganization and thus avoids the stabilization of the more polar charge-separated excited state (rigidochromic effect).[25] Still, the comparison of the emission spectra at 77 K reveals a strong bathochromic shift of 3520 cm^{-1} relative to the non-cyclometalated RuNNN caused by the strong HOMO destabilization in RuNCN. The functionalization of the NCN ligand with the slightly electron-donating thiophene causes no further HOMO destabilization, which might be attributed to the dihedral angle of around 30° which diminishes the conjugation.[26] In contrast, the functionalization of the NCN ligand with electron-withdrawing groups results in a HOMO stabilization, and thus a blue shift of the emission maximum of about 1130 cm^{-1} with respect to RuNCN.

Functionalization of the tpy ligand with carboxylic acid esters or free carboxylic acids causes a LUMO stabilization and, as a consequence, a red-shifted absorption and emission. However, it was only possible to measure the emission spectra at 77 K for RuNCN-COOH, which is red-shifted by 490 cm^{-1} relative to RuNCN. We note that the detector is less sensitive in the near-infrared region as demonstrated by the response function in Figure 6. A theoretically predicted emission of RuNCN-$(COOMe)_3$ above 1000 nm (Table 1) would thus not be detectable with our measurement setup.

Another important excited-state parameter is its lifetime, which, in contrast to the emission quantum yield, truly reflects the stability of the excited state. Therefore, emission lifetimes were determined at both room temperature and 77 K (Table 1). As a main result, the emission lifetime decreases with decreasing emission energy. Assuming that thermally activated radiationless deactivation pathways are frozen at 77 K, this can be explained by the energy-gap law.[27] Usually, it can be observed only within a series of very similar complexes or in different solvents,[28] since other effects, such as delocalization and rigidity, may interfere so that long excited-state lifetimes and small energy gaps do not exclude each other.[29] Accordingly, RuNCN-COOH has a longer lifetime than RuNCN (Table 1), which is attributed to the modification of the acceptor ligand.

Temperature-dependent lifetime measurements: To gain detailed insight into the deactivation dynamics of the lowest-lying excited state and the stabilizing/destabilizing effects of different substitution patterns, temperature-dependent lifetime measurements were carried out between 300 and 160 K.[34] The results of these experiments are depicted in Figure 7.

In general, the investigated cyclometalated complexes reveal a steady rise of the emission lifetime with decreasing temperature. However, depending on the specific substitution pattern, the slope of the lifetime increase varies. Similar to the emission spectra at 77 K, the complexes RuNCN-F and RuNCN-NO_2 show a different behavior compared to RuNCN, RuNCN-Cbz, and RuNCN-Tph. In detail, for the last three complexes the lifetime starts to increase at higher temperatures and shows a reduced slope than for RuNCN-F and RuNCN-NO_2, thus being shorter-lived at 77 K. In accordance with the literature, the excited-state lifetime at higher temperatures is determined by thermal deactivation via ^{3}MC states.[1,2] Evidently, the electron-withdrawing groups reduce the donor strength of the carbanion and therefore lower the ^{3}MC states. Consequently, thermal deactivation is facilitated, which can be quantified by fitting an Arrhenius expression to the experimental data [Eqs. (1) or (2)]. Thus, fundamental information about thermally activated, non-radiative deactivation channels can be obtained, for example, their rate constants and activation energies.

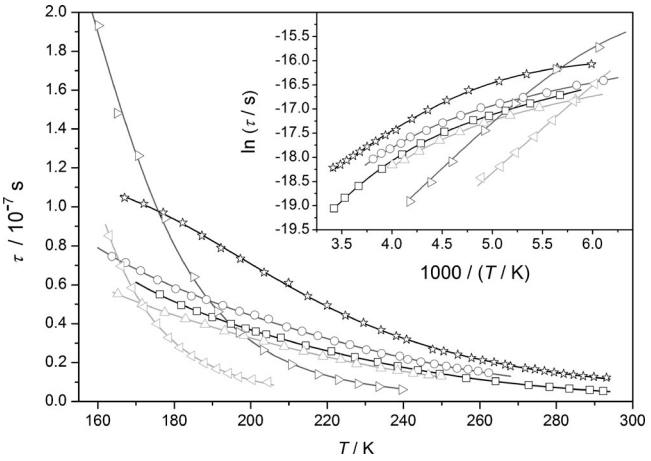

Figure 7. Temperature-dependent emission lifetimes for the complexes: RuNCN-F (◁), RuNCN-NO_2 (▷), RuNCN-Cbz (○), RuNCN (□), RuNCN-Tph (△) and RuNCN-COOH (☆) in *n*-butyronitrile. Symbols correspond to measured lifetimes and solid lines represent a non-linear fit according to equation 1 (RuNCN-COOH, RuNCN-F and RuNCN-NO_2) or equation 2 (RuNCN, RuNCN-Cbz and RuNCN-Tph). A color figure is given in the Supporting Information (Figure S120).

$$\tau(T) = \frac{1}{k_r + \sum k_{nr}} = \frac{1}{k_r + k_1 + k_2 \exp(-\Delta E_2/k_B T)} \quad (1)$$

$$\tau(T) = \frac{1}{k_r + \sum k_{nr}} = \frac{1}{k_r + k_1 + k_2 \exp(-\Delta E_2/k_B T) + k_3 \exp(-\Delta E_3/k_B T)} \quad (2)$$

For RuNCN, RuNCN-Cbz, and RuNCN-Tph, two thermally activated (k_2, ΔE_2 and k_3, ΔE_3) and one non-activated decay channel (k_1),[35] in addition to the radiative one (k_r), are necessary to fit the equation to the data [Eq. (2)]. In contrast, for RuNCN-F and RuNCN-NO_2 a model of three channels (a radiative, a non-activated, and a thermally activated non-radiative one) is sufficient to reproduce the data [Eq. (1)]. In principle, there should be a third dark channel for the last two complexes, but due to its low activation energy it is not visible in the experimental temperature

 © 2012 Wiley-VCH Verlag GmbH & Co. KGaA, Weinheim

range between 300 and 160 K. The results obtained by analyzing the temperature-dependent lifetime data are summarized in Table 1.

The first activated decay channel (k_2, ΔE_2) is assigned to the transition from the emitting ^{3}MLCT to the S_0 via the ^{3}MC excited state.[36] Compared to $[Ru(tpy)_2]^{2+}$ and other complexes of functionalized terpyridines, this activation energy is remarkably low (see the discussion of the ^{3}MC geometry in the DFT section).[30,34] We postulate that the room-temperature emission and prolonged excited-state lifetimes, which were observed despite similar or lower activation energies for the ^{3}MLCT–^{3}MC internal conversion than in $[Ru(tpy)_2]^{2+}$, are caused by a weaker coupling of the ^{3}MC and the ground state.[36] This is substantiated by small k_2 rate constants (10^{11}–10^{12} vs. 1.7×10^{13} s^{-1} in case of $[Ru(tpy)_2]^{2+}$). To the best of our knowledge, such a temperature-dependent excited-state lifetime measurement has been performed the first time for cyclometalated ruthenium(II) complexes. In principle, we would expect a similar behavior for $[Ru(tpy)(dpb)]^+$ or analogous complexes.

Furthermore, for RuNCN-F and RuNCN-NO_2 lower ΔE_2 values were obtained, supporting the assumption of a decreased ^{3}MC destabilization, but k_2 is again small and even smaller for RuNCN-NO_2. When comparing RuNCN-F and RuNCN-NO_2, the fluoro substituent mainly lowers the ^{3}MC energy, which is therefore closer to the ^{3}MLCT state. In contrast, the π-accepting nitro group *para* to the carbanion also affects the ^{3}MLCT energy (see the LUMO energy in Table 2) resulting in a larger observed ^{3}MLCT–^{3}MC barrier that allows for room-temperature emission. This is also reflected by the displacement of the RuNCN-F curve to lower temperatures (Figure 7).

Despite this good correlation between structure and excited-state dynamics, the temperature-dependent emission properties of RuNCN-COOH need to be discussed separately. Within the whole series, its activation energy for the ^{3}MLCT–^{3}MC internal conversion is the least. Nevertheless, a room-temperature lifetime of 12.3 ns could be measured, which is remarkably high in comparison with the other complexes discussed herein. This can only be explained by the relatively low transition rate for this process, which is one order of magnitude smaller than in the other complexes. Apparently, here the absence of a detectable room-temperature emission might be due to experimental limitations and does not necessarily mean short excited-state lifetimes.

The second activated decay channel (k_3, ΔE_3) can be attributed to internal conversion (IC) to an energetically slightly higher-lying MLCT state of increased singlet character (MLCT′), which is also a common feature for ruthenium polypyridyl dyes.[30,37]

Electrochemistry: Crucial for the potentially photo-redoxactive Ru^{II} complexes, in particular with respect to photovoltaic applications, are their electrochemical properties. Thus, the reversibility of the redox processes and the location of the oxidation and reduction potentials in comparison to the I_3^-/I^- couple and the TiO_2 conduction band, respectively, are highly important. Consequently, cyclic voltammetry (CV) measurements were carried out and related results are presented in Figures 8 and 9, Table 2, and the Supporting Information.

Analyzing the influence of cyclometalation by comparing RuNCN to RuNNN shows a strong cathodic shift of the oxidation potential of 900 mV due to the strong σ and π donation as well as electronic repulsion caused by the carbanion.[6a] Based on the calculations (see above), the first oxidation of RuNCN is not only metal-, but also ligand-based, and corresponds to a transition from d_{Ru}/π_{NCN}^{+} to $d_{Ru}/\pi_{NCN}^{2+\cdot}$ transition. Also the first reduction process, located on the terpyridine ligand, is shifted towards lower potentials by 260 mV, owing to increased π back donation from the more electron-rich Ru^{II} center.[5j] Both oxidation and reduction process of the RuNCN complex are fully reversible under cyclic voltammetric conditions. Nevertheless, reversibility was investigated in a more detailed fashion by UV/Vis spectroelectrochemical means (see below).

Again, a comparison of the triazole-containing complexes with their pyridine counterparts allows for a relative classification of electronic properties of the ligands. In comparison to the RuNNN-analogous $[Ru(tpy)_2][PF_6]_2$, the substitution of a terpyridine ligand by the click-derived 2,6-bis(1,2,3-triazol-4-yl)pyridine leads to a metal-based HOMO of lower energy and tpy-based LUMO of higher energy, indicating a weaker σ-donor and π-acceptor strength of the triazole-containing ligand that would allow the tpy to predominate the π back donation.[8a–d] In contrast, when comparing

Table 2. Electrochemical data of the complexes.

Complex	$E_{1/2}^{ox}$ [V] (i_{pa}/i_{pc}, ΔE_p [mV])[a]	$E_{1/2}^{red}$ [V] (i_{pa}/i_{pc}, ΔE_p [mV])[a]	E_{S*}(ox) [V][d]	E_{HOMO} [eV][c]	E_{LUMO} [eV][c]	$E_{gap,el}$ [eV]	$E_{gap,opt}$ [eV]
RuNNN	0.98 (1.1, 74)	−1.72 (0.9, 80)	−1.22	−5.78	−3.22	2.56	2.20
$[Ru(tpy)_2][PF_6]_2$[5j]	0.89 (64)	−1.66 (63)	–	–	–	–	–
RuNCN	0.08 (1.0, 67)	−1.98 (1.0, 71)	−1.83	−4.88	−2.91	1.97	1.91
$[Ru(tpy)(dpb)]PF_6$[5j]	0.12 (62)	−1.95 (63)	–	–	–	–	–
RuNCN-F	0.31 (1.0, 74)	−1.95 (1.0, 79)	−1.67	−5.12	−2.97	2.15	1.98
RuNCN-NO_2	0.26 (1.0, 76)	−1.82 (1.0, 88)	−1.77	−5.07	−3.11	1.96	2.03
RuNCN-Cbz	0.10 (1.0, 83)	−1.97 (irrev.)[b]	−1.84	−4.89	−3.00	1.89	1.94
RuNCN-Tph	0.07 (1.0, 69)	−1.97 (irrev.)[b]	−1.93	−4.87	−2.93	1.94	2.00
RuNCN-COOEt	0.16 (1.0, 70)	−1.79 (1.1, 80)	−1.74	−4.96	−3.14	1.82	1.90
RuNCN-$(COOMe)_3$	0.26 (1.0, 71)	−1.56 (1.0, 71)	−1.51	−5.06	−3.37	1.69	1.77

[a] Measured in CH_3CN with 0.1 M Bu_4NPF_6; with respect to Fc/Fc^+ as a reference. [b] Irreversible process; $E_{1/2}$ received from DPP. [c] Calculated by using $E_{LUMO/HOMO}=[-(E_{onset}^{red/ox}-E_{onset}^{Fc/Fc^+})-4.8]$ eV. [d] Calculated using $E_S=E_{1/2}^{ox}-E_{gap,opt}$.[3b]

© 2012 Wiley-VCH Verlag GmbH & Co. KGaA, Weinheim

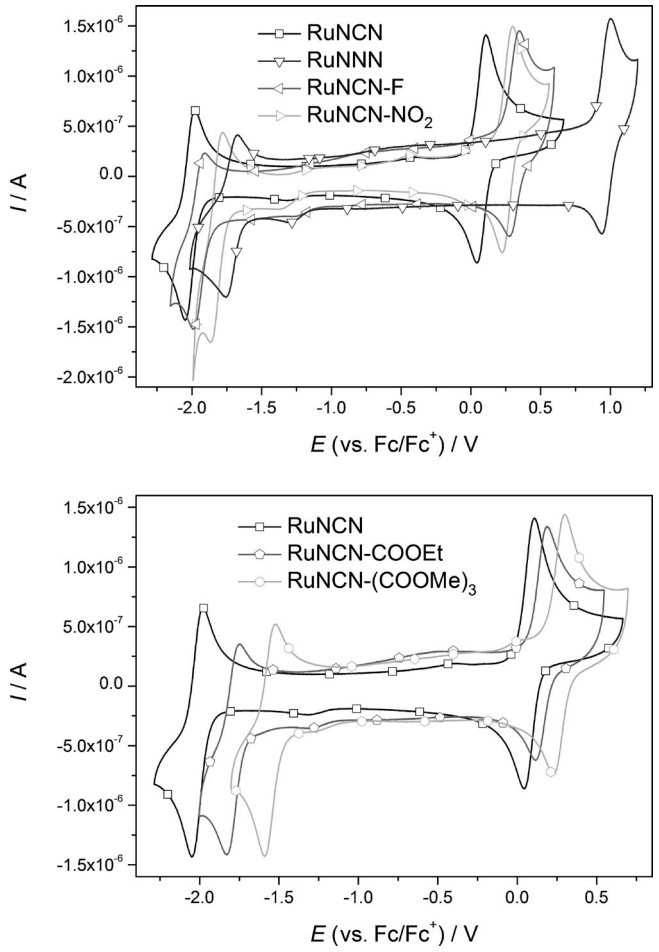

Figure 8. Cyclovoltammetric spectra of the cyclometalated ruthenium(II) complexes and RuNNN as a reference (10^{-5} M in CH_3CN with 0.1 M Bu_4NPF_6). Solid lines represent the measured curve and symbols are only used for assignment.

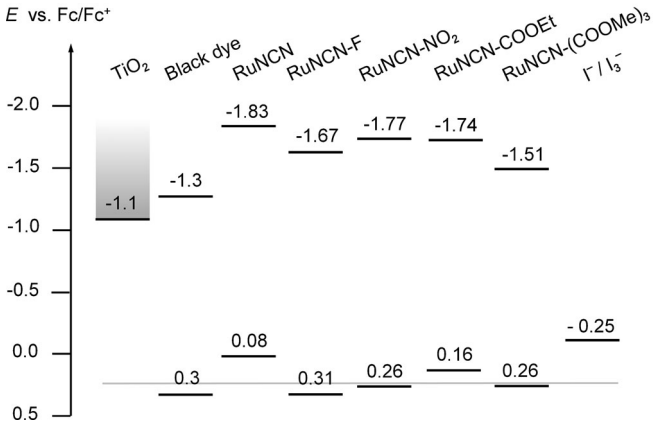

Figure 9. Comparison of the excited-state and ground-state oxidation potentials with the TiO_2 conducting band and the I^-/I_3^- redox couple, respectively. The grey line indicates a potential that ensures enough driving force for the dye regeneration.[3b,5i] The actual TiO_2 conducting band edge depends on the electrolyte composition and is therefore drawn diffusely.[38]

RuNCN with the analogous $[Ru(tpy)(dpb)]PF_6$, for the click-derived complex the oxidation and reduction potentials are cathodically shifted. Evidently, the triazole-containing cyclometalating ligand is a stronger π donor increasing the electron density on the Ru^{II}/NCN-based HOMO and, through increased π back donation from the more electron-rich Ru^{II} to the tpy ligand, the energy of the tpy-based LUMO. This is most likely due to weaker stabilization of the carbanion by the triazole in terms of its electron excess and shorter conjugation length.[8a] Additionally, for the same reason as for RuNNN, the lower π acceptor strength of the triazole-containing cyclometalating ligand, when compared to its pyridine analogue, might cause the HOMO and tpy-based LUMO of higher energy. Consequently, the more negative excited-state oxidation potential (Figure 9, Table 2) should increase the driving force for the electron injection into the TiO_2 conducting band or would allow for a higher TiO_2 conducting band, which can be achieved by a different electrolyte composition,[38] and therefore higher cell voltages. At the same time, the lower oxidation potential would lower the driving force for the regeneration of the photooxidized dye (Figure 9). In consistence with the blue shift of absorption and emission, which correspond to the optical gap, the electrochemical HOMO–LUMO gap of RuNCN is increased in comparison with $[Ru(tpy)(dpb)]PF_6$.

To still allow efficient dye regeneration, a fine-tuning of the oxidation potential was achieved by installing electron-withdrawing fluoro and nitro groups on the cyclometalated phenyl ring.[5c–e] Thus, the HOMO is stabilized and the oxidation shows an anodic shift by 230 and 180 mV, respectively, to be about 0.5 V more positive than the I^-/I_3^- redox couple and, thereby, ensure enough driving force for the dye reduction.[3b,5c,e,i,39] In the case of RuNCN-F, the reduction potential remains nearly unchanged, while for RuNCN-NO_2 a distinct anodic shift from −1.98 to −1.82 V is observed. Most likely, the strong π-accepting nitro group weakens the π donation of the *para*-carbanion and, thereby, the π back donation to the terpyridine. A more detailed discussion of the electronic effects of nitro and fluoro substituents on a cyclometalated phenyl ring depending on their positions can be taken from the literature.[5d,40]

Introduction of the carbazole and thiophene moieties affects the oxidation and reduction potentials only marginally, but leads to irreversibility of the reduction process under CV conditions in both cases. However, only the dye oxidation and subsequent reduction is the operative process in DSSCs and this process still is reversible. We note that a strategic methyl group was placed in the 5-position of the thiophene to avoid any following reactions, such as radical dimerizations.[41]

Electrochemical investigations on the ester-substituted complexes RuNCN-COOEt and RuNCN-$(COOMe)_3$ showed significant anodic shifts of the reduction potentials about 190 and 430 mV, respectively, due to stabilization of the LUMO, which is tpy-based. Still, enough driving force for a fast electron injection would be given. Furthermore, since the π-accepting esters are in *para* position, they in-

 © 2012 Wiley-VCH Verlag GmbH & Co. KGaA, Weinheim

crease the overall π-acceptor strength of the polypyridyl ligand, causing a small anodic shift of the oxidation of 80 and 180 mV, respectively. Thus, the oxidation potential of RuNCN-$(COOMe)_3$ would enable efficient regeneration. However, the strongly electron-withdrawing carboxylic ester can only be seen as approximation of TiO_2-adsorbed carboxylic acids[5k] and the actual electronic situation depends on the protonation state of the adsorbed complex (see pK_a determinations in the Supporting Information).[42] Therefore, although electron-withdrawing, the anchoring carboxylic acids most likely will have to be combined with above-mentioned strategies to lower the oxidation potential directly.[5c,e,i] Consequently, the RuNCN complexes are basically applicable in established DSSCs.

UV/Vis spectroelectrochemical analysis: To obtain a more detailed insight into the electrochemistry of the presented cyclometalated Ru^{II} systems, mainly with regard to reversibility and redox stability, UV/Vis spectroelectrochemical experiments were performed (see Figure 10 for RuNCN and Figures S122–S128 in the Supporting Information for the remaining complexes).

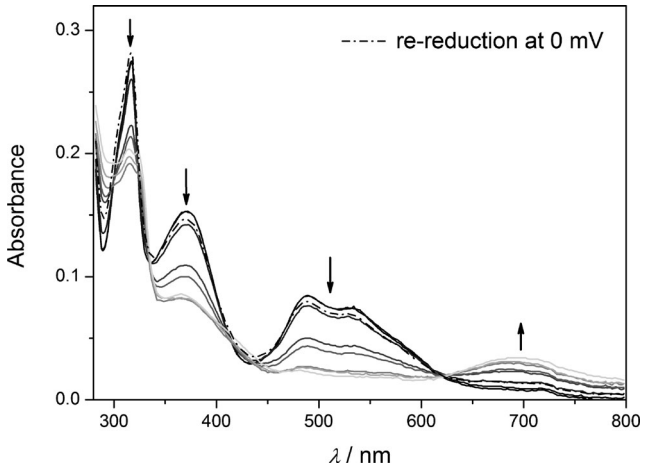

Figure 10. UV/Vis spectroelectrochemical investigation on the oxidation process of RuNCN (voltage varied between 400 and 1000 mV vs. Ag/AgCl; 10^{-5} M in CH_3CN with 0.1 M Bu_4NPF_6).

In general, the oxidation processes show several isosbestic points, indicating the temporary presence of only two species to ultimately form the singly oxidized complex in a well-defined reaction. The most evident changes during oxidation are the decrease of MLCT and MLLCT bands between 350 and 600 nm, caused by depopulation of the d_{Ru}/π_{NCN} HOMO, and the appearance of additional, broad peaks between 600 and 850 nm (up to 1000 nm in case of RuNCN-$(COOMe)_3$), most likely attributed to emerging LMCT ($\pi_{NCN}\rightarrow d_{Ru}$) or LMLCT ($\pi_{NCN}\rightarrow d_{Ru}/\pi_{NCN}$) transitions. Here, the fluoro-substituted RuNCN-F represents an exception that shows no changes beyond 600 nm (Figure S123 in the Supporting Information), probably because of a very low transition dipole moment. Accordingly, for RuNCN-NO_2 the arising transition is very weak. In contrast, the thiophene-containing complex RuNCN-Tph exhibits the appearance of two intense absorption peaks around 450 and 900 nm (Figure S126 in the Supporting Information), which can be likely assigned to a mixed MC/MLCT (MMLCT, $d_{Ru}\rightarrow d_{Ru}/\pi_{NCN}$), MLCT ($d_{Ru}\rightarrow\pi^*_{NCN}$), or LMLCT transitions that would possess large orbital contributions of the thiophene. Remarkably, the reductions of all oxidized species recreate the original spectra almost completely, thus confirming that the oxidation processes are fully reversible even under these demanding conditions under which the complexes are oxidized for a long time.

The first reductions (studied only for the complexes showing reversible reduction under CV conditions, see the Supporting Information), being located on the terpyridine ligand ($tpy\rightarrow tpy^{\bullet-}$), reveal a less-defined spectral change in spectroelectrochemical measurements. Again, an absorbance decrease in the MLCT/MLLCT region can be observed, caused by the population of a π^*_{tpy} orbital that acts as the acceptor within the longest-wavelength transition processes. Additionally, the absorbance also increases at around 450 nm and several changes occur in the UV region of the spectrum, both originating from appearing, disappearing, or shifted LC and LLCT transitions. In contrast to the oxidation described above, recreation of the initial complex is not successful in most cases, which is likely due to following reactions. As an exception, RuNCN-$(COOMe)_3$, which possesses three electron-withdrawing ester groups at the terpyridine ligand that enable an enhanced stabilization of the electron-rich $tpy^{\bullet-}$ moiety, allows the nearly full regeneration by re-oxidation.

Photophysical model: Cyclometalated polypyridyl Ru^{II} complexes have been known for some time,[6,9a] but it was only quite recently that they have been applied to the field of dye-sensitized solar cells.[5] Although there has been elaborated research on photoactive electron-transfer assemblies, such as homo- and heteronuclear dyads, for the prototypical bis(tridentate), heteroleptic Ru^{II} complex of terpyridine and its cyclometalated analogue 1,3-dipyridylbenzene, a detailed investigation on the excited-state processes is missing up to date.[32,43] Only a simplified, qualitative explanation of its photophysical properties by relative energies of the S_0, the lowest ^{3}MLCT state and the ^{3}MC state has been reported.[6a,32] According to that, the lifetime of the charge-separated excited-state is determined by the ^{3}MLCT–^{3}MC energy difference, since the metal-centered excited state shows a strong coupling to the ground state and therefore causes a rapid relaxation once the ^{3}MC state is populated. This is plausible because antibonding orbitals are occupied in the ^{3}MC state, which shows a displacement that typically matches the ground-state geometry at high-energy vibrations; in other words, the transition is highly probable because of a large Franck–Condon factor (strong coupling case of displaced oscillators).[44] Alternatively, the fast decay to the ground state can be explained in a classical picture assuming the surfaces show a nearly barrierless crossing.[45]

 © 2012 Wiley-VCH Verlag GmbH & Co. KGaA, Weinheim

However, we emphasize that the $^3MC–S_0$ intersystem crossing not only depends on the ^3MC, but also on the S_0 potential energy surface, which itself is strongly influenced by the electronic nature of the ligand. Thus, several Ru^{II} complexes have been reported, for example, $Ru(bpy)_2(CN)_2$, that show a weaker $^3MC–S_0$ coupling.[36] Despite these studies, the prolonged excited-state lifetime of the cyclometalated [Ru(tpy)(dpb)]$^+$ in comparison to $[Ru(tpy)_2]^{2+}$ has only been attributed to the ^3MC destabilization by the carbanion so far.

Nonetheless, temperature-dependent emission lifetime measurements reveal a similar and even lowered activation barrier for the population of the ^3MC state within the RuNCN series compared to $[Ru(tpy)_2]^{2+}$. At the same time, the non-radiative deactivation rate constant of RuNCN is orders of magnitude smaller than for $[Ru(tpy)_2]^{+}$.[30] We expect a similar behaviour for the analogous [Ru(tpy)(dpb)]$^+$ complex.

Consequently, Δ-SCF calculations were performed to gain a deeper understanding of the photophysics. In Figure 11 the schematic potential energy surfaces for the complexes RuNCN and RuNNN are depicted. The diabatic energies (DE) are obtained as the energetic differences between the energy minima of the optimized geometries, while the adiabatic energies (AE) are obtained as the actual energy differences at the ^3MLCT and the ^3MC optimized geometries. As shown in Figure 11, the ^3MLCT and ^3MC minima are almost

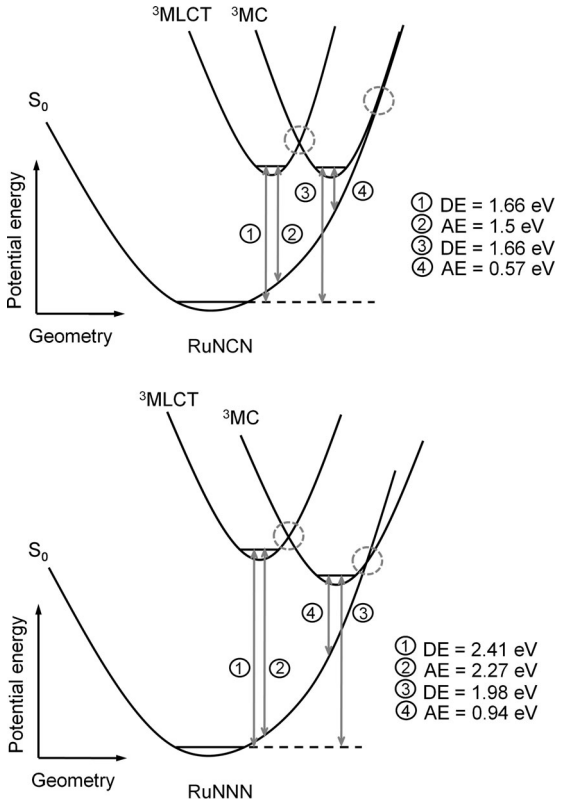

Figure 11. Proposed potential energy surfaces (the MLCT′ is omitted for clarity) including adiabatic (AE) and diabatic energies (DE) at the ΔSCF-PCM-DFT/6-31G* level of theory for the complexes RuNCN (top) and RuNNN (bottom).

isoenergetic for RuNCN, while for RuNNN the ^3MC minimum is lower in energy than the ^3MLCT one. This is in agreement with a destabilized ^3MC state for RuNCN as a result of the cyclometalation. As an additional consequence, the S_0 is destabilized as well and both ^3MLCT and ^3MC states appear at lower energies relative to the S_0. However, for the thermal $^3MLCT–^3MC$ internal conversion, the energy barrier and the respective $^3MLCT–^3MC$ conversion rate (see ΔE_2 and k_2 in the temperature-dependent lifetime measurements) are determining. Usually, the subsequent $^3MC–S_0$ intersystem crossing rate is the limiting rate. Thus, referring to the experimental $^3MLCT–^3MC$ energy barrier, which is lower for RuNCN than for $[Ru(tpy)_2]^{2+}$, and the nonetheless prolonged excited-state lifetimes, we postulate a weaker $^3MC–S_0$ coupling. In agreement with previous reports,[46] we conclude that the $^3MC–S_0$ intersystem crossing occurs at high energies on the potential energy surfaces for RuNCN, while for RuNNN and $[Ru(tpy)_2]^{2+}$ this $^3MC–S_0$ intersystem crossing point is at low energies and thus readily accessible. This is plausible, since the covalent binding of the cyclometalating ligand has a significant influence on both electronic structure and geometry already of the S_0 affecting also the $^3MC–S_0$ coupling.

Still, the lifetime of cyclometalated complexes is relatively short and the quantum yield is low in comparison to $[Ru(bpy)_3]^{2+}$, for example, because of the S_0 destabilization. The resulting small $S_0–^3MLCT$ energy gap leads to a more probable thermally non-activated, radiationless deactivation due to an increased Franck–Condon overlap of the S_0 and ^3MLCT vibrational wave functions. The observed decrease of the excited-state lifetime with decreasing emission energy is in accordance with the already mentioned energy-gap law.[27]

Conclusion

A systematically modified series of new ruthenium(II) complexes of click-derived tridentate cyclometalating ligands aimed towards the application in dye-sensitized solar cells was investigated. An optimized synthetic route was established. The presented cyclometalated ruthenium(II) polypyridyl complexes feature all benefits of established Ru^{II} thiocyanate dyes:

1) The HOMO is raised in energy causing a small energy gap and, therefore, a strongly red-shifted absorption.
2) The strong electron donation destabilizes ^3MC states and thus offers prolonged excited-state lifetimes.
3) The HOMO is extended to the cyclometalating ligand that facilitates the dye regeneration.
4) The LUMO is located on the opposite, anchoring ligand. Consequently, the charge transfer is directed towards the semiconductor surface.
5) At the same time, the anchoring groups, namely the carboxylic acid functions, strongly lower the LUMO energy, resulting in a panchromatic shift and intense absorption

 © 2012 Wiley-VCH Verlag GmbH & Co. KGaA, Weinheim

due to the pronounced push–pull effect that heightens the oscillator strengths and the extinction coefficients.

Additionally, the cyclometalated complexes offer further advantages that are essentially absent in thiocyanate complexes:

6) The electronic functions of the monodentate thiocyanate ligands are adopted by a multidentate ligand thus preventing photochemical ligand loss and offering higher long-term stability.
7) Since the HOMO is extended to the cyclometalating ligand, the optoelectronic properties can be optimized by ligand functionalization. Thus, redox-matching with the electrolyte and improvement of the light harvesting are enabled.

Moreover, the complexes of triazole-containing tridentate cyclometalating ligands offer potential advantages over their pyridyl analogues:

8) The stronger effective electron donation allows for longer excited-state lifetimes.
9) Their ligands can be readily and modularly functionalized.

A potential drawback might be the lower extinction coefficients, although strategies to increase them have been demonstrated. Still, the determined optoelectronic properties strongly encourage us to test the presented type of complex in a dye-sensitized solar cell. Also, a potential iodide–triazole interaction shall be investigated in the future.

As a result of the combined efforts of experimental and computational methods, a detailed understanding of the photophysical properties is provided, in particular of the crucial radiationless deactivation process of cyclometalated ruthenium(II) complexes.

Experimental Section

Extensive experimental details are given in the Supporting Information. These include synthetic procedures, UV/Vis absorption and emission, CV, NMR and ESI-Tof MS spectra, further solid-state structures and a more detailed discussion thereof, as well as computational details. CCDC-848606 (HNCN), CCDC-848607 (HNCN-F), CCDC-848608 ([Ru(tpy)(CH_3CN)$_3$][PF_6]$_2$), CCDC-848609 ([Ru(tpy-COOEt)(CH_3CN)$_3$][PF_6]$_2$), CCDC-848610 ([Ru(tpy-(COOMe)$_3$)(CH_3CN)$_3$][PF_6]$_2$), CCDC-848611 (RuNNN), CCDC-848612 (RuNCN), CCDC-848613 (RuNCN-NO_2), CCDC-848614 (RuNCN-F), and CCDC-848615 (RuNCN-Tph) contain the supplementary crystallographic data for this paper. These data can be obtained free of charge from The Cambridge Crystallographic Data Centre via www.ccdc.cam.ac.uk/data_request/cif.

Acknowledgements

Financial support by the Thuringian Ministry for Education, Science and Culture (grant no. B514-09049: Photonische Mizellen, PhotoMIC) is kindly acknowledged. B.S., C.F., and R.S. are grateful to the Fonds der Chemischen Industrie for Ph.D. scholarships. D.E. is grateful to the DAAD for financial support. B.D. and J.P. thank the Fonds der Chemischen Industrie. We also thank M. Jäger, E. Altuntas, W. Günther and G. Sentis for discussions and performing experiments. Additionally, we thank D. Schrader, S. Ziemann, and J. Türker for experimental assistance.

[1] a) A. Juris, V. Balzani, F. Barigelletti, S. Campagna, P. Belser, A. von Zelewsky, *Coord. Chem. Rev.* **1988**, *84*, 85–277; b) J. P. Sauvage, J. P. Collin, J. C. Chambron, S. Guillerez, C. Coudret, V. Balzani, F. Barigelletti, L. De Cola, L. Flamigni, *Chem. Rev.* **1994**, *94*, 993–1019.
[2] a) L. Hammarström, O. Johansson, *Coord. Chem. Rev.* **2010**, *254*, 2546–2559; b) E. A. Medlycott, G. S. Hanan, *Chem. Soc. Rev.* **2005**, *34*, 133–142; c) E. A. Medlycott, G. S. Hanan, *Coord. Chem. Rev.* **2006**, *250*, 1763–1782.
[3] a) B. O'Regan, M. Grätzel, *Nature* **1991**, *353*, 737–740; b) A. Hagfeldt, G. Boschloo, L. Sun, L. Kloo, H. Pettersson, *Chem. Rev.* **2010**, *110*, 6595–6663.
[4] a) M. K. Nazeeruddin, A. Kay, I. Rodicio, R. Humphry-Baker, E. Mueller, P. Liska, N. Vlachopoulos, M. Grätzel, *J. Am. Chem. Soc.* **1993**, *115*, 6382–6390; b) M. K. Nazeeruddin, P. Péchy, T. Renouard, S. M. Zakeeruddin, R. Humphry-Baker, P. Comte, P. Liska, L. Cevey, E. Costa, V. Shklover, L. Spiccia, G. B. Deacon, C. A. Bignozzi, M. Grätzel, *J. Am. Chem. Soc.* **2001**, *123*, 1613–1624; c) H. Tributsch, *Coord. Chem. Rev.* **2004**, *248*, 1511–1530.
[5] a) P. G. Bomben, K. C. D. Robson, P. A. Sedach, C. P. Berlinguette, *Inorg. Chem.* **2009**, *48*, 9631–9643; b) B. D. Koivisto, K. C. D. Robson, C. P. Berlinguette, *Inorg. Chem.* **2009**, *48*, 9644–9652; c) T. Bessho, E. Yoneda, J.-H. Yum, M. Guglielmi, I. Tavernelli, H. Imai, U. Rothlisberger, M. K. Nazeeruddin, M. Grätzel, *J. Am. Chem. Soc.* **2009**, *131*, 5930–5934; d) P. G. Bomben, B. D. Koivisto, C. P. Berlinguette, *Inorg. Chem.* **2010**, *49*, 4960–4971; e) P. G. Bomben, K. D. Thériault, C. P. Berlinguette, *Eur. J. Inorg. Chem.* **2011**, 1806–1814; f) K. C. D. Robson, B. D. Koivisto, A. Yella, B. Sporinova, M. K. Nazeeruddin, T. Baumgartner, M. Grätzel, C. P. Berlinguette, *Inorg. Chem.* **2011**, *50*, 5494–5508; g) K. C. D. Robson, B. Sporinova, B. D. Koivisto, E. Schott, D. G. Brown, C. P. Berlinguette, *Inorg. Chem.* **2011**, *50*, 6019–6028; h) S. H. Wadman, J. M. Kroon, K. Bakker, M. Lutz, A. L. Spek, G. P. M. van Klink, G. van Koten, *Chem. Commun.* **2007**, 1907–1909; i) P. G. Bomben, T. J. Gordon, E. Schott, C. P. Berlinguette, *Angew. Chem.* **2011**, *123*, 10870–10873; *Angew. Chem. Int. Ed.* **2011**, *50*, 10682–10685; j) S. H. Wadman, M. Lutz, D. M. Tooke, A. L. Spek, F. Hartl, R. W. A. Havenith, G. P. M. van Klink, G. van Koten, *Inorg. Chem.* **2009**, *48*, 1887–1900; k) S. H. Wadman, J. M. Kroon, K. Bakker, R. W. A. Havenith, G. P. M. van Klink, G. van Koten, *Organometallics* **2010**, *29*, 1569–1579.
[6] a) J.-P. Collin, M. Beley, J.-P. Sauvage, F. Barigelletti, *Inorg. Chim. Acta* **1991**, *186*, 91–93; b) E. C. Constable, J. M. Holmes, *J. Organomet. Chem.* **1986**, *301*, 203–208.
[7] H. C. Kolb, M. G. Finn, K. B. Sharpless, *Angew. Chem.* **2001**, *113*, 2056–2075; *Angew. Chem. Int. Ed.* **2001**, *40*, 2004–2021.
[8] a) Y. Li, J. C. Huffman, A. H. Flood, *Chem. Commun.* **2007**, 2692–2694; b) R. M. Meudtner, M. Ostermeier, R. Goddard, C. Limberg, S. Hecht, *Chem. Eur. J.* **2007**, *13*, 9834–9840; c) M. Ostermeier, M.-A. Berlin, R. M. Meudtner, S. Demeshko, F. Meyer, C. Limberg, S. Hecht, *Chem. Eur. J.* **2010**, *16*, 10202–10213; d) B. Schulze, C. Friebe, M. D. Hager, A. Winter, R. Hoogenboom, H. Görls, U. S. Schubert, *Dalton Trans.* **2009**, 787–794; e) B. Happ, C. Friebe, A. Winter, M. D. Hager, R. Hoogenboom, U. S. Schubert, *Chem. Asian J.* **2009**, *4*, 154–163; f) B. Schulze, D. Escudero, C. Friebe, R. Siebert, H. Görls, U. Köhn, E. Altuntas, A. Baumgaertel, M. D. Hager, A. Winter, B. Dietzek, J. Popp, L. González, U. S. Schubert, *Chem. Eur. J.* **2011**, *17*, 5494–5498.
[9] a) M. Beley, J. P. Collin, R. Louis, B. Metz, J. P. Sauvage, *J. Am. Chem. Soc.* **1991**, *113*, 8521–8522; b) J. A. G. Williams, *Chem. Soc. Rev.* **2009**, *38*, 1783–1801; c) B. Beyer, C. Ulbricht, D. Escudero, C.

 © 2012 Wiley-VCH Verlag GmbH & Co. KGaA, Weinheim

Friebe, A. Winter, L. González, U. S. Schubert, *Organometallics* **2009**, *28*, 5478–5488.

[10] While this manuscript was in preparation, a communication by Zhong, Yao et al. already introduced this type of click-derived NCN-cyclometalated Ru^{II} complex. However, only a basic characterization was provided and the synthesis was not optimized. W.-W. Yang, L. Wang, Y.-W. Zhong, J. Yao, *Organometallics* **2011**, *30*, 2236–2240.

[11] Very recently, the use of a 1,2,3-triazolylpyridine within a classical Ru^{II}–thiocyanate complex demonstrated the potential of a click-derived ligand for solar-cell applications. I. Stengel, A. Mishra, N. Pootrakulchote, S.-J. Moon, S. M. Zakeeruddin, M. Grätzel, P. Bauerle, *J. Mater. Chem.* **2011**, *21*, 3726–3734.

[12] A. J. Wilkinson, H. Puschmann, J. A. K. Howard, C. E. Foster, J. A. G. Williams, *Inorg. Chem.* **2006**, *45*, 8685–8699.

[13] C. Amatore, A. Jutand, *Acc. Chem. Res.* **2000**, *33*, 314–321.

[14] J. G. Rodríguez, T. Laparra, *Tetrahedron* **2009**, *65*, 2551–2555.

[15] a) C. Y. Chen, H. C. Lu, C. G. Wu, J. G. Chen, K. C. Ho, *Adv. Funct. Mater.* **2007**, *17*, 29–36; b) C. Y. Chen, S. J. Wu, J. Y. Li, C. G. Wu, J. G. Chen, K. C. Ho, *Adv. Mater.* **2007**, *19*, 3888–3891; c) C.-Y. Chen, J.-G. Chen, S.-J. Wu, J.-Y. Li, C.-G. Wu, K.-C. Ho, *Angew. Chem.* **2008**, *120*, 7452–7455; *Angew. Chem. Int. Ed.* **2008**, *47*, 7342–7345; d) C.-Y. Chen, S.-J. Wu, C.-G. Wu, J.-G. Chen, K.-C. Ho, *Angew. Chem.* **2006**, *118*, 5954–5957; *Angew. Chem. Int. Ed.* **2006**, *45*, 5822–5825; e) C.-C. Chou, K.-L. Wu, Y. Chi, W.-P. Hu, S. J. Yu, G.-H. Lee, C.-L. Lin, P.-T. Chou, *Angew. Chem.* **2011**, *123*, 2102–2106; *Angew. Chem. Int. Ed.* **2011**, *50*, 2054–2058; f) F. Gao, Y. Wang, D. Shi, J. Zhang, M. Wang, X. Jing, R. Humphry-Baker, P. Wang, S. M. Zakeeruddin, M. Grätzel, *J. Am. Chem. Soc.* **2008**, *130*, 10720–10728; g) F. Gao, Y. Wang, J. Zhang, D. Shi, M. Wang, R. Humphry-Baker, P. Wang, S. M. Zakeeruddin, M. Grätzel, *Chem. Commun.* **2008**, 2635–2637; h) N. Hirata, J.-J. Lagref, E. J. Palomares, J. R. Durrant, M. K. Nazeeruddin, M. Gratzel, D. Di Censo, *Chem. Eur. J.* **2004**, *10*, 595–602.

[16] R. Westlund, E. Glimsdal, M. Lindgren, R. Vestberg, C. Hawker, C. Lopes, E. Malmström, *J. Mater. Chem.* **2008**, *18*, 166–175.

[17] a) M. Jäger, R. J. Kumar, H. Görls, J. Bergquist, O. Johansson, *Inorg. Chem.* **2009**, *48*, 3228–3238; b) H. F. Suen, S. W. Wilson, M. Pomerantz, J. L. Walsh, *Inorg. Chem.* **1989**, *28*, 786–791.

[18] M. Gagliardo, D. J. M. Snelders, P. A. Chase, R. J. M. Klein Gebbink, G. P. M. van Klink, G. van Koten, *Angew. Chem.* **2007**, *119*, 8710–8726; *Angew. Chem. Int. Ed.* **2007**, *46*, 8558–8573.

[19] a) Y. Li, A. H. Flood, *Angew. Chem.* **2008**, *120*, 2689–2692; *Angew. Chem. Int. Ed.* **2008**, *47*, 2649–2652; b) Y. Li, A. H. Flood, *J. Am. Chem. Soc.* **2008**, *130*, 12111–12122; c) S. Liu, P. Müller, M. K. Takase, T. M. Swager, *Inorg. Chem.* **2011**, *50*, 7598–7609; d) B. Schulze, C. Friebe, M. D. Hager, W. Günther, U. Köhn, B. O. Jahn, H. Görls, U. S. Schubert, *Org. Lett.* **2010**, *12*, 2710–2713.

[20] L. González, D. Escudero, L. Serrano-Andrés, *ChemPhysChem.* **2012**, *13*, 28–51.

[21] a) B. Happ, D. Escudero, M. D. Hager, C. Friebe, A. Winter, H. Görls, E. Altuntaş, L. González, U. S. Schubert, *J. Org. Chem.* **2010**, *75*, 4025–4038; b) A. Vlček Jr., S. Záliš, *Coord. Chem. Rev.* **2007**, *251*, 258–287; c) M.-F. Charlot, A. Aukauloo, *J. Phys. Chem. A* **2007**, *111*, 11661–11672.

[22] J. Heully, F. Alary, M. Boggio-Pasqua, *J. Chem. Phys.* **2009**, *131*, 184308.

[23] a) K. C. D. Robson, B. D. Koivisto, T. J. Gordon, T. Baumgartner, C. P. Berlinguette, *Inorg. Chem.* **2010**, *49*, 5335–5337; b) R. Siebert, A. Winter, B. Dietzek, U. S. Schubert, J. Popp, *Macromol. Rapid Commun.* **2010**, *31*, 883–888.

[24] R. Englman, J. Jortner, *Mol. Phys.* **1970**, *18*, 145–164.

[25] a) F. Barigelletti, P. Belser, A. Von Zelewsky, A. Juris, V. Balzani, *J. Phys. Chem.* **1985**, *89*, 3680–3684; b) M. Wrighton, D. L. Morse, *J. Am. Chem. Soc.* **1974**, *96*, 998–1003.

[26] a) M. Presselt, B. Dietzek, M. Schmitt, J. Popp, A. Winter, M. Chiper, C. Friebe, U. S. Schubert, *J. Phys. Chem. C* **2008**, *112*, 18651–18660; b) M. Presselt, B. Dietzek, M. Schmitt, S. Rau, A. Winter, M. Jäger, U. S. Schubert, J. Popp, *J. Phys. Chem. A* **2010**, *114*, 13163–13174.

[27] a) J. V. Caspar, T. J. Meyer, *J. Phys. Chem.* **1983**, *87*, 952–957; b) K. R. Barqawi, Z. Murtaza, T. J. Meyer, *J. Phys. Chem.* **1991**, *95*, 47–50; c) J. V. Caspar, E. M. Kober, B. P. Sullivan, T. J. Meyer, *J. Am. Chem. Soc.* **1982**, *104*, 630–632.

[28] J. V. Caspar, B. P. Sullivan, E. M. Kober, T. J. Meyer, *Chem. Phys. Lett.* **1982**, *91*, 91–95.

[29] J. A. Treadway, B. Loeb, R. Lopez, P. A. Anderson, F. R. Keene, T. J. Meyer, *Inorg. Chem.* **1996**, *35*, 2242–2246.

[30] A. C. Benniston, G. Chapman, A. Harriman, M. Mehrabi, C. A. Sams, *Inorg. Chem.* **2004**, *43*, 4227–4233.

[31] M. Abrahamsson, M. Jäger, R. J. Kumar, T. Österman, P. Persson, H.-C. Becker, O. Johansson, L. Hammarström, *J. Am. Chem. Soc.* **2008**, *130*, 15533–15542.

[32] M. Beley, S. Chodorowski, J.-P. Collin, J.-P. Sauvage, L. Flamigni, F. Barigelletti, *Inorg. Chem.* **1994**, *33*, 2543–2547.

[33] C. R. Hecker, A. K. I. Gushurst, D. R. McMillin, *Inorg. Chem.* **1991**, *30*, 538–541.

[34] a) R. Siebert, C. Hunger, J. Guthmuller, F. Schlütter, A. Winter, U. S. Schubert, L. González, B. Dietzek, J. Popp, *J. Phys. Chem. C* **2011**, *115*, 12677–12688; b) R. Siebert, A. Winter, U. S. Schubert, B. Dietzek, J. Popp, *Phys. Chem. Chem. Phys.* **2011**, *13*, 1606–1617.

[35] As a non-radiative temperature-independent channel is assumed to contribute to the excited-state dynamics the experimental phosphorescence rate at 77 K can be expressed as $1/\tau_{77K} = k_r + k_1$.

[36] a) G. H. Allen, R. P. White, D. P. Rillema, T. J. Meyer, *J. Am. Chem. Soc.* **1984**, *106*, 2613–2620; b) W. F. Wacholtz, R. A. Auerbach, R. H. Schmehl, *Inorg. Chem.* **1986**, *25*, 227–234; c) F. Barigelletti, A. Juris, V. Balzani, P. Belser, A. Von Zelewsky, *J. Phys. Chem.* **1987**, *91*, 1095–1098; d) A. Islam, N. Ikeda, A. Yoshimura, T. Ohno, *Inorg. Chem.* **1998**, *37*, 3093–3098.

[37] a) B. J. Coe, D. W. Thompson, C. T. Culbertson, J. R. Schoonover, T. J. Meyer, *Inorg. Chem.* **1995**, *34*, 3385–3395; b) R. S. Lumpkin, E. M. Kober, L. A. Worl, Z. Murtaza, T. J. Meyer, *J. Phys. Chem.* **1990**, *94*, 239–243; c) M. Sykora, J. R. Kincaid, *Inorg. Chem.* **1995**, *34*, 5852–5856; d) H. Yersin, E. Gallhuber, A. Vogler, H. Kunkely, *J. Am. Chem. Soc.* **1983**, *105*, 4155–4156.

[38] B. Enright, G. Redmond, D. Fitzmaurice, *J. Phys. Chem.* **1994**, *98*, 6195–6200.

[39] G. Boschloo, A. Hagfeldt, *Acc. Chem. Res.* **2009**, *42*, 1819–1826.

[40] Z. Wang, E. Turner, V. Mahoney, S. Madakuni, T. Groy, J. Li, *Inorg. Chem.* **2010**, *49*, 11276–11286.

[41] J. Heinze, B. A. Frontana-Uribe, S. Ludwigs, *Chem. Rev.* **2010**, *110*, 4724–4771.

[42] Y. Tachibana, M. K. Nazeeruddin, M. Grätzel, D. R. Klug, J. R. Durrant, *Chem. Phys.* **2002**, *285*, 127–132.

[43] M. Beley, J. P. Collin, J. P. Sauvage, *Inorg. Chem.* **1993**, *32*, 4539–4543.

[44] K. Freed, J. Jortner, *J. Chem. Phys.* **1970**, *52*, 6272–6291.

[45] J. H. Alstrum-Acevedo, M. K. Brennaman, T. J. Meyer, *Inorg. Chem.* **2005**, *44*, 6802–6827.

[46] I. M. Dixon, F. Alary, J.-L. Heully, *Dalton Trans.* **2010**, *39*, 10959–10966.

Received: November 3, 2011
Published online: February 29, 2012

 © 2012 Wiley-VCH Verlag GmbH & Co. KGaA, Weinheim